Pyrolysis and combustion of community masks: Thermogravimetric analyses, characterizations, gaseous emissions, and kinetic modeling

Alain Brillard, Damaris Kehrli, Orlane Douguet, Karine Gautier, Valerie Tschamber, Marie-Ange Bueno, Jean-Francois Brilhac

Pyrolysis and combustion of community masks: thermogravimetric analyses, characterizations, gaseous emissions, and kinetic modeling

Alain Brillard[1,a], Damaris Kehrli[a], Orlane Douguet[a,b], Karine Gautier[b], Valérie Tschamber[a], Marie-Ange Bueno[b], Jean-François Brilhac[a]

[a] University of Haute-Alsace, Laboratoire de Gestion des Risques et Environnement (LGRE, UR 2334), Institut de Recherche Jean-Baptiste Donnet, 3bis rue Alfred Werner, 68093 Mulhouse Cedex, France

[b] University of Haute Alsace, Laboratoire de Physique et Mécanique Textiles (EAC 7189 CNRS/UHA), École Nationale Supérieure d'Ingénieurs Sud Alsace (ENSISA), 11 rue Alfred Werner, 68093 Mulhouse Cedex, France

Abstract

Used community masks are often thrown away or scattered in the environment. In addition to the unsightly aspect of such waste, these masks are a diffuse source of pollution because of some of their synthetic components: polypropylene, polyethylene terephthalate (PET), polyamide 6, polyamide 66, and elastane. These diffuse sources of pollution must be processed in an appropriate way, once they are collected. Among such processes, pyrolysis or combustion are to be explored.

In the present study, five different masks were characterized before being submitted to pyrolysis and combustion experiments performed in a thermobalance under temperature ramps of 5, 10, 15, or 20 °C/min. Kinetic modeling of these pyrolysis or combustion processes was performed using the EIPR model because each mask contains different layers or components. The optimal values of the kinetic parameters were compared for the five masks and compared with that of their components. In complement to the thermogravimetric experiments, the main gaseous emissions (CO, CO_2, THC, NO

[1] Corresponding author
Alain.Brillard@uha.fr

and NO_2) were continuously measured during combustion tests in a horizontal oven. The gaseous emissions and mass rates curves were compared for each mask.

Keywords

Community mask; Pyrolysis; Combustion; Kinetic modeling; Gaseous emissions

1. Introduction

With the propagation of the COVID-19 pandemic, governments throughout the world encourage or impose to their citizens wearing community masks. Companies throughout the world were encouraged to manufacture community masks with either knitted or nonwoven fabrics made with natural or synthetic fibers. The world production of community masks was largely increased because of this increasing demand. In the European Economic Area, surgical masks have to be certified through the CE marking process before commercialization, according to the Council Regulation 2017/745 concerning medical devices, [1].

Community masks can be machine washed a number of times indicated in their instructions for use. Once this limit is reached, the degradable and used community masks should be disposed in a biohazardous-waste bin, being disposed in a first bag. Other community masks should be disposed in classical waste bins and they are then treated like domestic waste. However, everyone can find community masks along the streets, in the landscape, the rivers or even the seas. Uplifting photos of used community masks found in different sites are presented in [2] and on Peruvian beaches in [3], as examples.

Recycling community masks is surely complicated, as they are made with different components. Several recycling processes were tested, see the recent review [4] for example. In the recent paper [5], the authors explored the possibility to consider used community masks for pavement base or

subbase. Thermal conversions (essentially pyrolysis) of community masks are being explored, either on the whole mask [4], [6], or with other medical waste [7], [8], [9]. The pyrolysis of a surgical mask rope built with 5% polyurethane spandex and 95% polyamide 6 was analyzed in [10].

The purpose of the present study is to analyze the thermal degradations of five community masks, four of them being manufactured in Alsace, North-East of France, and the fifth one being a surgical mask. The possibility to produce energy from such waste, through pyrolysis or combustion processes under low temperature ramps and keeping under control the emitted gases, is analyzed.

Different characterizations of the five community masks were first performed and compared with that of their natural or synthetic components.

Pyrolysis and combustion experiments were performed under four temperature ramps of 5, 10, 15, and 20 °C/min. The main characteristics of the degradation profiles are presented and compared and also compared to results of the literature concerning the natural or synthetic fibers. Kinetic modeling was performed for these pyrolysis or combustion processes, applying the Extended Independent Parallel Reaction (EIPR) model, [11]. The number of constituents to be considered in the EIPR model is adapted to each mask observing the mass and mass rate curves of the pyrolysis experiments. The reaction functions involved in the EIPR model are also adapted to these pyrolysis profiles. The optimal values of the kinetic parameters determined for each mask are compared to that indicated in the literature for its constituents.

In complement to these pyrolysis and combustion processes, combustion experiments were performed in a horizontal oven under a temperature ramp approximately equal to 5 °C/min. The main gaseous emissions (CO, CO_2, NO, NO_2, and total hydrocarbons THC) were continuously measured during these combustion experiments. The results obtained for the five masks are compared. For each mask, the evolution of the mass rate in the thermobalance under a temperature ramp of 5 °C/min is finally compared to that of the gaseous emissions measured in the horizontal oven.

The five community masks present a structure and a composition which differ in the nature of the fibers which are used for their elaboration. Consequently, their characteristics and thermogravimetric profiles slightly differ and also differ from that of the pure fibers they are made with.

The study presents a complete analysis of the thermal degradations under nitrogen and under air of five community masks built with different natural or synthetic fibers, and of the gaseous emissions occurring under combustion, together with a kinetic modeling of these thermal degradations.

2. Materials and Methods

2.1. Materials and characterizations

For the present study, five community masks were selected because of their current extensive use in France. Their structure, manufacturing process and components are the following:

- Single-layered and nonwoven mask, hereafter named BPET (70% polyethylene terephthalate, 30% polyamide 6).
- Three-layered and knitted mask, hereafter named ECLT (100% cotton / flax yarns / mixture of cotton, flax and Lyocell). The overall composition of the ECLT mask is: cotton 57%, flax 33% and Lyocell 10%). Lyocell is an artificial fiber made from cellulose, through the dissolution of pulp and reconstitution by dry jet-wet spinning. Consequently, the ECLT mask is totally made from cellulosic fibers.
- Single-layered and knitted fabric mask, hereafter named LCPE (70% cotton, 28% polyamide, 2% elastane).
- Three-layered mask, hereafter named MCP3 (knitted 100% fabric cotton / non-knitted evolon (microfibers made with 70% polyethylene terephthalate, 30% polyamide) / knitted 100% polyamide 66), that is a nonwoven microfibrous layer between two knitted layers.

- Three-layered nonwoven surgical mask, hereafter named SGP2 (100% polypropylene, a meltblown layer placed between two spunbond layers). Meltblown is obtained through extrusion of molten polymer under a hot air flow leading to very thin filaments. Spunbond is obtained from polymer through extrusion and drawing into coarser filaments deposited as a web. The surgical mask is the most widely used in many countries.

The first four masks were manufactured in Alsace, France, the last one being manufactured mainly in Asian countries. As indicated, ECLT is totally composed of cellulosic fibers, LCPE is mostly composed of cotton fibers, the three other masks being mostly or totally composed of synthetic fibers which are eventually treated before the mask fabrication.

Before their commercialization, community masks have first to be tested to satisfy national or international standards concerning filtration and air permeability properties. In France, the official specification AFNOR SPEC S76-001 [12], updated in January 2021, gives the threshold of 90% for filtration of particles of diameter equal to or lower than 3 µm. From January 2021, a unique category UNS1 (Non-Sanitary Usage) of masks is indeed considered. The air permeability properties with respect to air of community masks have to be greater than 96 L/(m^2.s) as indicated in the standards NF EN 14683+AC [13], or NF EN ISO 9237 [14]. The properties of the selected five masks are gathered in Table 1.

Table 1. Filtration and permeability properties of the five community masks.

	BPET	ECLT	LCPE	MCP3	SGP2
Filtration for particles of size 3 µm (%)	85	86	85	98	>98
Permeability to air, under depression at 100 Pa (L/(m^2.s))	152	231	411	116	>100

Only the two last selected masks satisfy the requirements imposed by the French regulation from January 2021 for the UNS1 category. The three first community masks are still used in the daily life.

Figure 1 presents photos of the five masks considered in the present study.

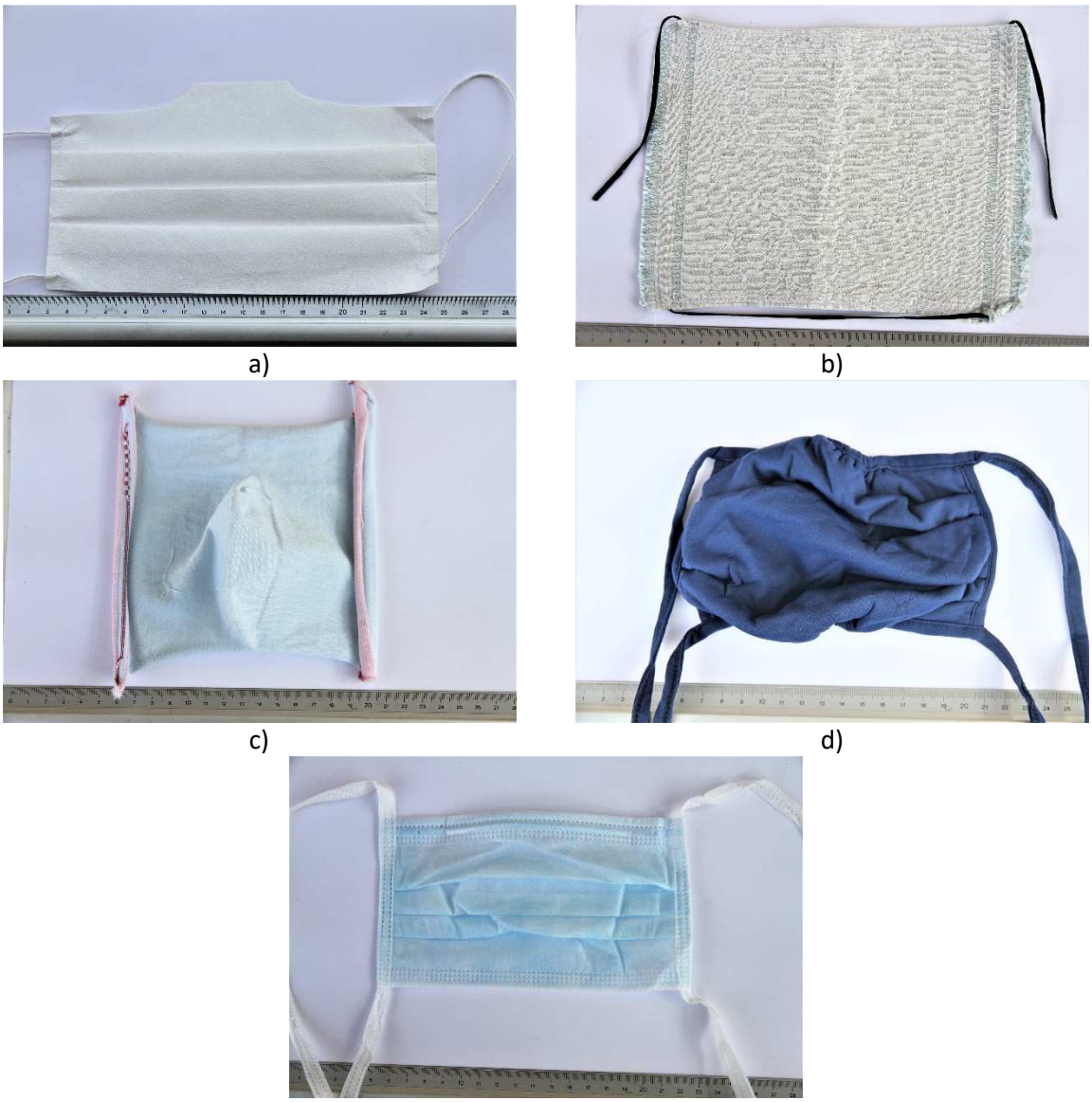

Fig.1. Photos of the BPET a), ECLT b), LCPE c), MCP3 d), and SGP2 e) community masks, with their ropes.

Only the characterizations and thermal degradations of the complete five masks will be performed and analyzed in the present study (and not that of their individual layers, even if thermogravimetric experiments and characterizations were also performed on some layers of the selected masks). The first reason is that, in most cases, separating the layers of a mask is not an easy task. On another aspect, performing such a separation has surely no sense from an economic point of view, if the valorization of the used mask consists to perform pyrolysis or combustion processes. Finally, the

layers and also the mask rope whose pyrolysis is considered in [10], are all built with the same natural or synthetic fibers (polyethylene terephthalate, polyamide 6, polyamide 66, polypropylene, cotton, flax and Lyocell). Nevertheless, pyrolysis and combustion experiments were also performed on individual components of the masks to analyze the observed thermogravimetric profiles of the masks.

The proximate analysis of each mask was performed using standard techniques and according to ISO 1171 [15] and EN NF 18122 [16] standards for biomass samples. The moisture content (M) was determined placing the sample in a Memmert VM400 oven at 105±2 °C for 24 hours, the sample mass remaining almost constant after this time length. The fixed carbon (FC) and volatile matter (VM) contents were determined comparing the initial and final masses of the samples submitted to pyrolysis and combustion experiments. A Nabertherm muffle furnace was used to determine the ash content of the masks at 815 °C, according to NF EN ISO 18122 [16].

The higher heating value (HHV) of each mask was determined placing the raw sample in a metal crucible in a calorimeter IKA C200 (accuracy 0.1 mg). Three measures of the HHV were performed. The lower heating value (LHV) was deduced from the HHV, according to the formula:

$$LHV = HHV - L_v\left(\frac{M}{100} + \frac{M_{H_2O}H}{200M_H}\right), \qquad (1)$$

where L_v=2486 kJ/kg is the latent heat of water vaporization at 273 K, *M* is the moisture content (%) determined in the proximate analysis, M_{H_2O}=18 g/mol is the water molar mass, M_H=1 g/mol is the hydrogen molar mass and *H* is the percentage of hydrogen in the sample determined in the ultimate analysis.

Ultimate analyses were performed in triplicate for each mask with an automatic elemental analyzer (EuroVector EA-3000) and according to ISO 29541 [17], ISO 19579 [18] and ASTM 3176-15 [19] standards. An ultimate analysis is based on the sample combustion followed by separation in a gas chromatography column and detection of the combustible products using a high sensitive catharometric detector.

153 The atomic ratios H/C and O/C were calculated according to Van Krevelen's formulas [20]:

154 $$H/C = \frac{\frac{\%H}{1/NA}}{\frac{\%C}{12/NA}}; O/C = \frac{\frac{\%O}{16/NA}}{\frac{\%C}{12/NA}} \qquad (2)$$

155 where %H, %C and %O are the percentages of H, C and O determined in the ultimate analysis and *NA*
156 is the Avogadro number (*NA* = 6.02×10^{23} atoms per mol).

157

158 *2.2. Thermogravimetric experiments*

159 Thermogravimetric experiments were performed for each complete community mask under pure
160 nitrogen or under air (80% nitrogen and 20% oxygen) in a thermobalance TA Q500, Texas Instrument.
161 A small piece (approximately 5-6 mg) of the fabrics part of each complete mask was placed in the
162 alumina pan of the thermobalance, Fig. 2.

163

164 Fig. 2. Installation of the samples (here from a SGP2 mask) in the pans of the TA Q500 thermobalance
165 for a thermogravimetric experiment.

166

167 Four low temperature ramps were applied (5, 10, 15, and 20 °C/min). The gas flow was held fixed at
168 50 mL/min. The temperature was increased from room temperature to 900 °C, but the thermal

degradations were finished before 700 °C. Each pyrolysis and combustion experiment was repeated at least three times for each mask, with good agreement.

2.3. Gaseous emissions during combustion

Combustion experiments were performed on the fabrics part of the five community masks in a horizontal tubular Nabertherm oven inside which was placed an alumina reactor of length 1 m and diameter 57 mm. A mask sample (0.2 to 0.5 g depending on the mask) was placed in an alumina boat and manually introduced at room temperature into the isothermal zone of the reactor. An air flow was then injected with a flow rate of 100 Nl/h. The temperature was increased from room temperature to 900 °C with a temperature ramp between 5.4 and 5.7 °C/min. CO, CO_2, NO, NO_2, and total hydrocarbons (THC) emissions at the outlet of the reactor were continuously measured using a multi-component NGA2000 Rosemount analyzer, with a flame-ionization detector or an infrared cell (for the NO emissions). Such a gaseous analyzer usually detects chemical compounds only with a number of carbon atoms lower than 10. Three experiments were performed for each mask.

2.4. Kinetic modeling through the EIPR model

The EIPR model is especially dedicated to the simulation of the thermal degradation of a material when this thermal degradation presents successive stages, for example, when the material is a lignocellulosic one, [11]. In the EIPR model, each stage is supposed to correspond to the thermal degradation of a constituent of the material and the thermal degradations of the constituents are supposed to occur in an independent way, but possibly in superimposing temperature ranges. The number of constituents to be considered in the EIPR model is determined observing the mass and mass rate curves. The EIPR model allows simulating the experimental mass and mass rate curves through the resolution of a system of first-order ordinary differential equations.

193

194 *2.4.1. Kinetic modeling through the EIPR model in the case of a non-oxidative atmosphere*

195 In the case of a non-oxidative atmosphere, the EIPR model consists in a set of ordinary differential
196 equations, whose number is equal to the number of constituents to be taken into account, each
197 equation describing the evolution of the mass of volatiles which are emitted from a constituent of
198 the material. Each first-order ordinary differential equation is written as:

199 $$\frac{dm_{vol,i}^{e}}{dt}(t) = k_i\big(T(t)\big) f\left(m_i(0) - m_{vol,i}^{e}(t)\right), i = 1, \dots, I, \quad (3)$$

200 where:

201 - $m_{vol,i}^{e}(t)$ is the mass of volatiles emitted from the constituent *i* of the sample (*i*=1,…,*I*),
202 - $m_i(0)$ is the initial mass of the constituent *i*, which may be computed as a fraction of the
203 overall mass of the sample: $m_i(0) = c_i\, m(0)$,
204 - f is a reaction function,
205 - $T(t)$ is the temperature (expressed in K) at time *t* in the sample. In the present experiments,
206 the temperature $T(t)$ evolves with respect to the time parameter *t* with a constant rate:
207 $T(t) = at + T_0$.

208 The initial value $m_{vol,i}^{e}(0) = 0$ is imposed.

209 For each mask, the number *I* of constituents to be considered in the EIPR model may be different
210 from that of its components, as some components may present a quite similar thermal degradation
211 profile.

212 In most cases, a first-order reaction function, or Mampel's reaction function, with respect to the
213 extent of conversion α, may be considered: $f_1(\alpha) = 1 - \alpha$, whatever the constituent of each
214 sample. In the present study, a second- or fourth-order Avrami-Erofeev reaction function with

respect to the extent of conversion α will also be considered for few constituents, which are respectively defined as:

$$f_2(\alpha) = 2(1-\alpha)(-\log(1-\alpha))^{1/4};\ f_4(\alpha) = 4(1-\alpha)(-\log(1-\alpha))^{3/4}\,. \quad (4)$$

Such Avrami-Erofeev reaction functions simulate in a better way the case of an intense devolatilization process, corresponding to a thin and high peak in the mass rate curve.

In the right-hand side of the equation (3), the kinetic constant $k_i(T)$ obeys an Arrhenius law: $k_i(T) = A_i \exp(-Ea_i/RT)$, where A_i (resp. Ea_i) is the pre-exponential factor (resp. the activation energy) for the constituent *i* and *R* is the ideal gas constant equal to 8.314 J/(mol.K).

In the present study, the system of differential equations (3) is solved using the Scilab software (version 6.0.2) and especially its routine 'ode', first with initial guesses of the kinetic parameters. The system (3) is solved simultaneously for the four temperature ramps. The optimal values of the kinetic parameters are then determined using the routine 'datafit' of Scilab, that is minimizing with respect to these kinetic parameters the objective function chosen as the sum over the four temperature ramps of the sum of the squared differences between the experimental and simulated mass rates:

$$\sum_{j=1}^{J}\left(\left(\frac{dm^e_{vol,i}}{dt}\right)_{exp}(t_j) - \left(\frac{dm^e_{vol,i}}{dt}\right)_{sim}(t_j)\right)^2, \quad (5)$$

where $\left(\frac{dm^e_{vol,i}}{dt}\right)_{exp}(t_j)$ is the experimental mass rate at time t_j and $\left(\frac{dm^e_{vol,i}}{dt}\right)_{sim}(t_j)$ is the simulated mass rate at time t_j, as deduced from the resolution of (3), for each temperature ramp. For each temperature ramp, the total number *J* of time points t_j was taken equal to 400 to reduce the computation time, these time points t_j being regularly distributed along the overall duration of the thermogravimetric experiment.

Once the optimal values of the kinetic parameters are determined, the system (3) is solved to obtain the simulated sample mass and mass rate as functions of time according to:

$$m(t) = m(0) - \sum_{i=1}^{I} m_{vol,i}^{e}(t), \qquad (6)$$

$$\frac{dm}{dt}(t) = \sum_{i=1}^{I} \frac{dm_{vol,i}^{e}(t)}{dt}, \qquad (7)$$

for each temperature ramp. This allows comparing the experimental and simulated mass and mass rate curves of the material, and simultaneously for the four temperature ramps.

To validate the simulations, the maximal difference $max_j \left| \left(\frac{dm_{vol,i}^{e}}{dt}\right)_{exp}(t_j) - \left(\frac{dm_{vol,i}^{e}}{dt}\right)_{sim}(t_j) \right|$, hereafter denoted l_∞, and the square root $\left(\sum_{j=1}^{J} \left(\left(\frac{dm_{vol,i}^{e}}{dt}\right)_{exp}(t_j) - \left(\frac{dm_{vol,i}^{e}}{dt}\right)_{sim}(t_j) \right)^2 \right)^{1/2}$ of (5), hereafter denoted l_2, between the experimental and simulated mass rates are calculated for each temperature ramp. For each temperature ramp, R^2 determination coefficients are also calculated for the mass according to the formula:

$$R_m^2 = 1 - \frac{\sum_{j=1}^{J} \left(m_{sim}(t_j) - m_{exp}(t_j) \right)^2}{\sum_{j=1}^{J} \left(m_{exp}(t_j) - \frac{1}{J} \sum_{k=1}^{J} m_{exp}(t_k) \right)^2}, \qquad (8)$$

where $m_{sim}(t_j)$ and $m_{exp}(t_j)$ are the simulated and experimental masses at time t_j. Quite similar formulas may be built for the mass rate and for the overall variations, whose expressions are given in the Supplementary Material. These determination coefficients should be as close to 1 as possible to validate the simulations.

2.4.2. Kinetic modeling through the EIPR model in the case of an oxidative atmosphere

Under an oxidative atmosphere, the devolatilization stages of the material surely occur. But the char structure is also degraded. The EIPR model considers that the constituents of the material lead to both the emission of volatiles and to the apparition of the char structure, once the volatiles are being

emitted, this char structure being degraded at higher temperatures. The fraction of volatiles to be emitted from the constituent *i* is denoted as $\tau_{vol,i}$. The complement of $\tau_{vol,i}$ to 1 represents the fraction of char which appears from the constituent *i* during the devolatilization stage and which will be degraded during the further combustion stage.

Under an oxidative atmosphere, the EIPR model first simulates the evolution of the mass of volatiles which are emitted from the constituent *i* of the material with respect to time according to the first-order ordinary differential equation:

$$\frac{dm_{vol,i}^{e}}{dt}(t) = k_i\big(T(t)\big)\left(m_i(0) - \frac{m_{vol,i}^{e}(t)}{\tau_{vol,i}}\right), i = 1, \dots, I, \quad (9)$$

where:

- $m_{vol,i}^{e}(t)$ is the mass of volatiles emitted by the constituent *i* of the sample (*i*=1,…,*I*),
- $m_i(0)$ is the initial mass of the constituent *i*, which may be computed as a fraction of the overall mass of the sample: $m_i(0) = c_i\, m(0)$,
- $T(t)$ is the temperature at time *t* in the sample (expressed in K) and which evolves with respect to the time parameter *t* with a constant rate: $T(t) = at + T_0$,
- $\tau_{vol,i}$ is the fraction of volatiles contained in the constituent *I* and which will be emitted during the devolatilization stage, as previously exposed. This fraction $\tau_{vol,i}$ has to be determined for each constituent of each mask, which is not an easy task. In the present study, this fraction is estimated observing the mass rate curves obtained from the thermal degradation of each mask under an oxidative atmosphere.

The presence of the fraction $\tau_{vol,i}$ of volatiles emitted by the constituent *i* of the sample is the unique difference between the equations (3) and (9).

The initial value $m_{vol,i}^{e}(0) = 0$ is imposed.

In the above equation (9), the kinetic constant k_i obeys an Arrhenius law: $k_i(T) = A_i \exp(-Ea_i/RT)$, where A_i (resp. Ea_i) is the pre-exponential factor (resp. the activation energy) for the devolatilization of the constituent *i*.

The evolution with respect to time of the mass $m^c_{char,i}$ of char which appears during the devolatilization of the constituent *i* and which is consumed is described according to the first-order ordinary differential equation:

$$\frac{dm^c_{char,i}}{dt}(t) = k_{comb}\big(T(t)\big)\left(\frac{1-\tau_{vol,i}}{\tau_{vol,i}} m^e_{vol,i}(t) - m^c_{char,i}(t)\right) P_{O_2}, \quad (10)$$

where the kinetic constant $k_{comb}(T)$ obeys an Arrhenius law: $k_{comb}(T) = A_{comb} exp(-Ea_{comb}/RT)$ and where P_{O_2} is the oxygen pressure which is constant during the experiment ($P_{O_2} = 2.1 \times 10^4$ Pa). The initial value $m^c_{char,i}(0) = 0$ is imposed. The kinetic constant k_{comb} is the same for the combustion of the chars produced from all constituents of each mask.

The system (9)-(10) is solved with a procedure adapted from that described in section 2.4.1 for the pyrolysis case and which is described in the Supplementary Material.

3. Results and discussion

3.1. Proximate and ultimate analyses of the complete community masks

The results of the proximate analyses performed on the five masks are gathered in Table 2.

Table 2. Proximate analysis, HHV and LHV, for the five complete masks.

Sample	Proximate analysis (%) as received				HHV (kJ/kg)[a]	LHV (kJ/kg)[b]
	M	FC	VM	Ash		
BPET	2.1±0.5	11.7±0.3	85.9±0.6	0.3±0.0	23636±419	22239±438
ECLT	7.4±0.1	9.9±0.2	82.5±0.5	0.2±0.1	16397±93	14749±100
LCPE	4.9±0.1	10.6±0.2	84.3±0.6	0.2±0.1	21164±367	19279±373
MCP3	4.6±0.2	7.5±0.1	87.3±0.7	0.6±0.1	21697±1428	19382±1436
SGP2	5.0±0.1	1.9±0.2	92.9±0.7	0.2±0.0	45345±151	41880±174

[a] on raw basis; [b] on dry and ash free basis

Whatever the mask, the percentage of volatiles is very high and the percentage of ash is very low. The percentage of volatiles of the SGP2 mask is slightly higher and its percentage of fixed carbon is much lower than that of the other masks. The ECLT mask which is totally composed of natural fibers (cotton and flax) has the lowest volatile matter percentage and the highest moisture percentage. For the volatile matter percentage, the ECLT mask is followed by the LCPE mask which also contains a high percentage of natural fibers (cotton).

The percentage of volatile matter was found higher than 99% for polypropylene samples in [21]. The percentage of volatile matter contained in a polypropylene sample was evaluated at 99.73% in [22]. The authors did not detect ash in their samples and the moisture content was very low.

The HHV of the SGP2 mask is twice higher than that of the other masks. It was also measured at around 45 MJ/kg in [23]. The ECLT mask which is totally composed of natural fibers has the lowest HHV. It is followed by the LCPE and by MCP3 masks which both contain natural fibers. The BPET mask has a HHV value slightly higher than these three masks, but half of that of the SGP2 mask, although it is also composed of synthetic fibers.

The ultimate analyses performed on the five masks return mean percentages over the three experiments gathered in Table 3 and whose sum is equal to 1 for each mask. From the different characterizations, the H/C and O/C ratios are computed through Eq. (2).

Table 3. Ultimate analysis, H/C and O/C ratios, for the complete five masks.

Sample	Ultimate analysis (%)					H/C ratio	O/C ratio
	C	H	O	N	S		
BPET	62.38±0.07	6.01±0.03	28.12±0.06	3.49±0.09	n.d.	1.16	0.34
ECLT	43.51±0.11	6.55±0.02	49.84±0.11	0.10±0.01	n.d.	1.81	0.86
LCPE	50.38±0.20	7.88±0.02	38.04±0.20	3.70±0.03	n.d.	1.88	0.57
MCP3	56.27±0.12	7.82±0.02	30.29±0.13	5.62±0.04	n.d.	1.67	0.40

SGP2	84.37±0.22	14.93±0.04	0.70±0.09	n.d.	n.d.	2.12	0.01

n.d. below detection.

For each mask, the sum of the mean percentages of C,H,N,O returned by the elemental analyzer is slightly less than 100%: 99.3% for BPET, 97,5% for ECLT, 96.7% for LCPE, 97.6 % for MCP3 and 99.9% for SGP2). The difference with 100% is more important for masks containing natural fibers (ECLT, LCPE and MCP3) than for masks made with synthetic fibers. Natural fibers indeed contain minerals.

The sulfur contents is below the detection limit for each mask. For the other elements, the masks present very high differences. Being totally composed of polypropylene (C_3H_6), the SGP2 mask does not contain nitrogen. High differences appear in the C percentages, as they represent between 43 and 62% of the overall mass for the first four masks and 84% for the SGP2 mask. These C percentages increase with the proportion of synthetic fibers. The H percentages lie between 6 and 8% for the first four masks but increases to 15% for the SGP2 one. Consequently, the O percentage is almost equal to 0% in the SGP2 mask, while it lies between 28 and 50% for the four other masks.

The C percentage was found equal to 85.7% in [21] for low-density polyethylene and polypropylene samples, slightly higher than that of the SGP2 mask, which is totally composed of polypropylene. The N, O, and S percentages were here indicated equal to 0. The C percentage was found equal to 85.11% in [22] for a polypropylene sample.

The values of the H/C and O/C ratios of the ECLT, LCPE and MCP3 masks are in good agreement with that of textiles. These values are lower for the BPET mask because of the higher C percentage of this mask. The values of these ratios for the SGP2 mask totally differ from those obtained for the four other masks. The SGP2 mask presents the highest H/C ratio because of its higher H percentage. It presents the lowest C/O ratio because of its very low O percentage.

3.2. Pyrolysis experiments under nitrogen of the complete community masks

The pyrolysis experiments performed on the fabrics part of the five complete masks lead to the mass and mass rate curves gathered in Fig. 3. For comparison between the masks, the sample masses are expressed in percentages and the percentages start at 100% at the beginning of the thermogravimetric experiment (approximately room temperature).

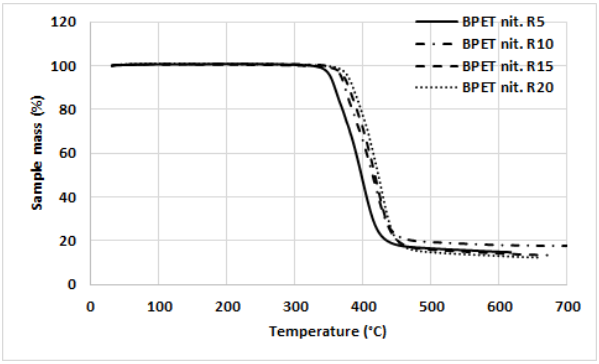

a)

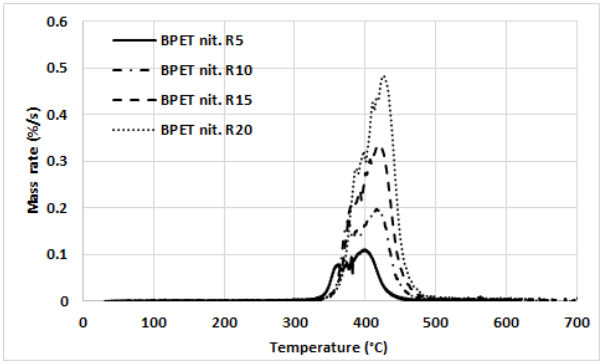

b)

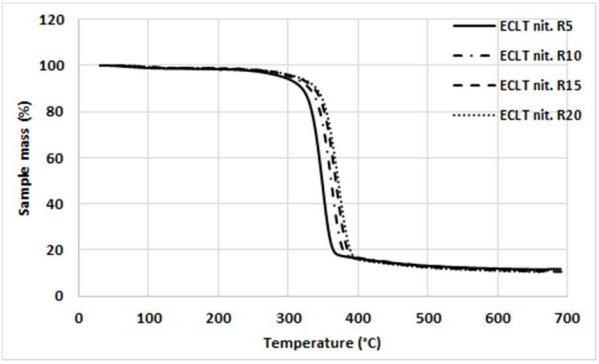

c)

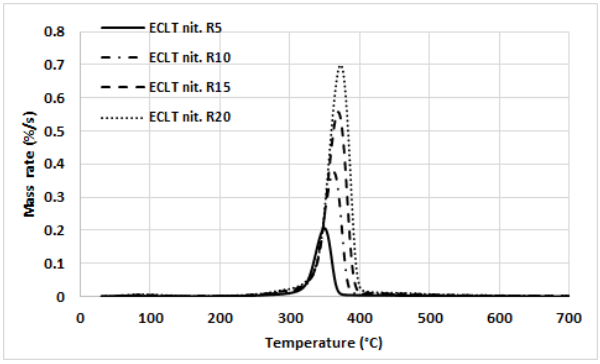

d)

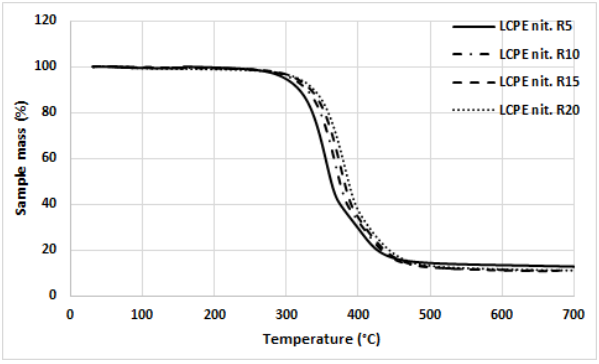

e)

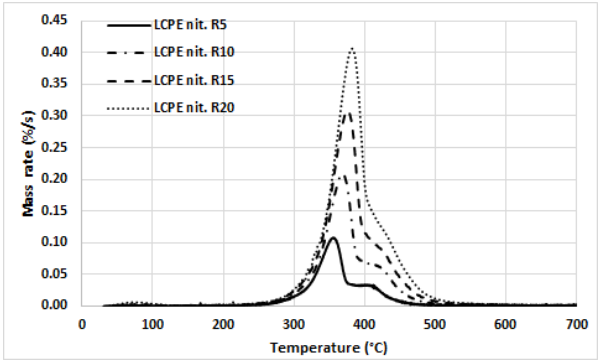

f)

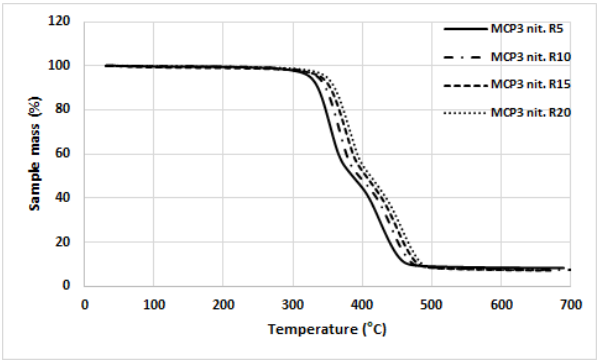

g)

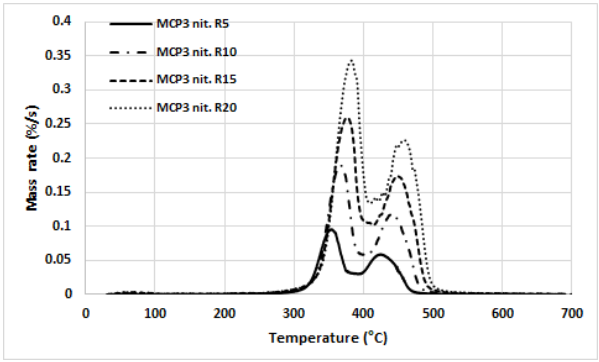

h)

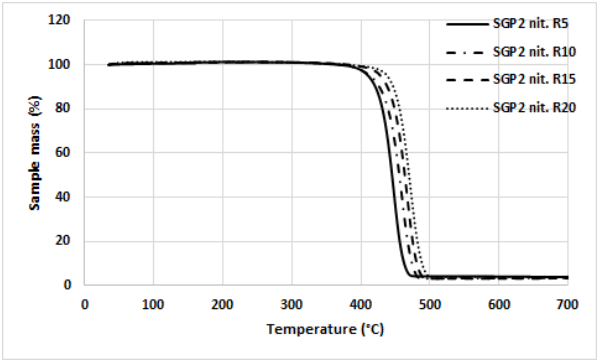

i)

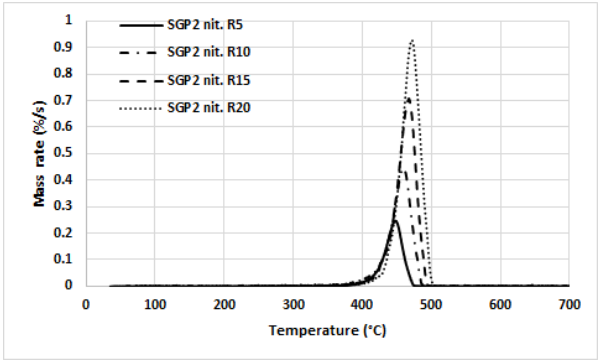

j)

Fig. 3. Mass curves for the pyrolysis of the complete BPET a), ECLT c), LCPE e), MCP3 g), and SGP2 i) masks. Mass rate curves for the pyrolysis of the complete BPET b), ECLT d), LCPE f), MCP3 h), and SGP2 j) masks. In each figure, the curves corresponding to a temperature ramp of 5 °C/min (resp. 10, 15, 20) are represented with a solid line (resp. large hyphened, small hyphened, and dotted lines).

The mass rate curves of ECLT, LCPE and MCP3 present a very small peak around 100 °C, which surely corresponds to the moisture evaporation. The mass rate curves of the two other masks do not present this small peak, although the moisture content of the SGP2 mask is comparable to that of LCPE and MCP3 masks.

The shapes of the mass and mass rate curves look very similar for each sample, whatever the temperature ramp, but they differ from one mask to another one:

- For the BPET mask, a unique devolatilization peak appears in the mass rate curves, with an important shoulder on the left-hand side of this peak. For the temperature ramps equal to 5 and 10 °C/min, these shoulders are close to peaks. This shape may be the consequence of the presence of two components (polyethylene terephthalate and polyamide 6), which are being decomposed in slightly different temperature ranges, see below.
- For the ECLT and SGP2 masks, a unique and thin peak appears on the mass rate curves. These masks are composed of a unique component (natural fibers for ECLT, almost totally composed of cellulose, and polypropylene for SGP2).
- For the LCPE mask, the mass rate curve obtained for the temperature ramp of 5 °C/min presents a first well-identified peak and a less important one on its right-hand side. For the other temperature ramps, the unique devolatilization peak presents an important shoulder on the right-hand side. This shape is the consequence of two major components: a natural fiber almost totally composed of cellulose, and a synthetic one, these components being degraded in slightly different temperature ranges.
- For the MCP3 mask, two well-identified peaks appear. This shape is the consequence of the presence of natural fibers which are being degraded at temperatures lower than 400 °C, see the thermogravimetric profile of the ECLT mask, and of synthetic fibers (polyethylene terephthalate and polyamides), which are being degraded at slightly higher temperatures, see the thermogravimetric profile of the BPET mask.
- The peaks of ECLT and SGP2 masks are very narrow, in comparison with that of the other masks.

For the five masks, the peaks which appear on the mass rate curves slightly shift to higher temperatures when the temperature rate increases, see also Table 4 for the positions of the peaks. The height of the peaks (highest mass rate) also increases with this temperature ramp.

Table 4. Position and height of each peak and final sample mass for the pyrolysis of the five complete masks.

Sample	First or main peak		Second peak		Final mass
	Temperature (°C)	Mass rate (%/s)	Temperature (°C)	Mass rate (%/s)	(%)
BPET					
R5	402.0	0.109	-	-	14.8
R10	422.3	0.196	-	-	17.9
R15	421.1	0.335	-	-	13.4
R20	425.9	0.483	-	-	12.3
ECLT					
R5	349.9	0.206	-	-	11.7
R10	363.1	0.377	-	-	11.1
R15	369.3	0.558	-	-	11.6
R20	373.1	0.699	-	-	10.5
LCPE					
R5	355.6	0.108	415.8	0.030	11.9
R10	368.7	0.209	-	-	11.1
R15	376.2	0.308	-	-	10.8
R20	382.4	0.406	-	-	14.2
MCP3					
R5	353.5	0.096	423.8	0.059	8.3
R10	366.7	0.190	439.7	0.118	9.4
R15	377.5	0.259	449.6	0.174	7.2
R20	382.3	0.343	459.1	0.226	7.3
SGP2					
R5	447.5	0.247	-	-	3.5
R10	460.3	0.445	-	-	4.1
R15	467.2	0.708	-	-	3.6
R20	471.5	0.929	-	-	4.2

The shifts to higher temperatures of the position of each peak, with respect to the temperature ramp, lie between 17 and 37 °C. There is no clear tendency of these shifts with respect to the components involved in the elaboration of the masks.

Whatever the mask the final masses do not obey a clear tendency with respect to the temperature ramp.

The slow pyrolysis of pure polyethylene terephthalate was performed in [24] under temperature ramps of 2, 5, 10, 20, and 30 °C/min. The authors found a unique devolatilization peak occurring at approximately 420, 440 and 450 °C, for temperature ramps equal to 5, 10 and 20 °C/min. In [10], the

390 pyrolysis of a surgical mask rope composed at 95% of polyamide 6 was performed under
391 temperature ramps of 5, 10 and 30 °C/min. The unique devolatilization peak was reached at 420 and
392 435 °C for the temperature ramps of 5 and 10 °C/min, respectively. The slow pyrolysis of polyamide
393 was performed in [25] under temperature ramps of 5, 10, 20, and 40 °C/min. The authors found a
394 unique devolatilization peak occurring at approximately 460, 475 and 490 °C. The slow pyrolysis of
395 polyamide 6 and polyamide 66 was performed in [26] under nitrogen and under a temperature ramp
396 of 10 °C/min. The authors found a unique peak at 436 and 430 °C, respectively. A small shoulder was
397 observed for polyamide 6 on the left-hand side of the peak. One reason which could explain the
398 possible slightly lower temperatures at which the peak for the pyrolysis of the BPET mask indicated in
399 Table 5 occur when comparing to that of the literature could be the mixture of polyethylene
400 terephthalate and polyamide 6 fibers in this mask.

401 The pyrolysis of used cotton fabric and of pure cellulose was analyzed in [27]. A heat transfer model
402 was here proposed to explain the shift and the increase of the devolatilization peak with respect to
403 the temperature ramp. The unique thin peak occurred at 349, 363 and 375 °C for the temperature
404 ramps of 5, 10 and 20 °C/min. The position of the peaks observed for the ECLT mask are in good
405 agreement with these values. For the present study, the pyrolysis of pure cotton and flax samples
406 were performed under a temperature ramp of 5 °C/min. The maximal mass rate occurred at 330 and
407 341 °C, respectively.

408 The two peaks observed for the pyrolysis of the MCP3 mask may surely be associated to that of
409 cotton, for the first peak, and to the pyrolysis of synthetic fibers (polyethylene terephthalate and
410 polyamide), for the second peak.

411 Pyrolysis experiments were performed in [28] on polypropylene pellets under temperature ramps of
412 4, 6, 8, and 10 °C/min. The authors claimed that the thermal degradations of polyethylene and
413 polypropylene occur in very similar ways, because of their composition, even if, "*due to the presence*
414 *of methyl groups of side chains, intramolecular hydrogen transfer is more preferable in degradation*

of PP than for PE". They observed a unique devolatilization peak approximately occurring at 450 °C for the temperature ramp of 10 °C/min. This value is to be compared to that (455 °C) obtained for the pyrolysis of SGP2 composed of polypropylene, under the temperature ramp of 10 °C/min. Pyrolysis experiments were performed on low-density polyethylene and polypropylene samples in [21], under temperature ramps of 5, 10, 15, and 20 °C/min. The authors did not present the mass rate curves, but their mass curves present a rapid decrease in the range 420-480 °C, for low-density polyethylene, and in the range 350-420 °C, for polypropylene. Pyrolysis experiments were performed in [29] on waste low-density polyethylene, waste polypropylene terephthalate and polypropylene, under a temperature ramp of 10 °C/min. The pyrolysis occurred in the temperature range 341-495 °C for low-density polyethylene, 329-493 °C for polyethylene terephthalate, and 337-471 °C for polypropylene. A unique devolatilization peak was observed for each material, with a maximum reached at 463, 437-441 and 446 °C, respectively. In [22], pyrolysis experiments were performed on polypropylene samples eventually in presence of activators and under temperature ramps of 15, 20, and 30 °C/min. The authors observed a very narrow peak whose maximal height is reached at approximately 480 and 490 °C for the temperature ramps of 15 and 20 °C/min.

The pyrolysis of Korean surgical masks built with polypropylene (73%), polyethylene (14%), nylon (8%), and metals (5%) was analyzed in [6] under a temperature ramp equal to 10 °C/min, together with that of these pure components. The authors found a unique devolatilization peak occurring at 450, 455 and 460 °C for polypropylene, whole mask and polyethylene. The peak temperature of 450 °C observed for polypropylene has to be compared to that of the SGP2 masks equal to 455.6 °C for the temperature ramp of 10 °C/min. Whatever the mask, the temperatures presented in Table 4 at which the mass rate reaches its maximum are in good agreement with that of the literature for pyrolysis experiments.

Especially paying attention to the peaks and shoulders which appear on the mass rate curves of Fig. 5, the number of constituents to be considered in the EIPR model is the following for each mask:

- BPET: 2, to be compared to the two components (polyethylene terephthalate and polyamide 6) used for its elaboration,
- ECLT: 1, to be compared to the three components (cotton, flax and Lyocell) used in its elaboration,
- LCPE: 3, to be compared to the three components (cotton, polyamide and elastane) used in its elaboration,
- MCP3: 2, to be compared to the four components (cotton, polyethylene terephthalate, polyamide, and polyamide 66) used in its elaboration,
- SGP2: 1, this mask being totally composed of polypropylene.

The differences between the numbers of constituents to be considered in the EIPR model and of components involved in the elaboration of each mask may be explained by the fact that some components are being degraded in a quite similar way and in quite superimposing temperature ranges.

The thinness of the unique peaks for ECLT and SGP2 masks requires the use of the second-order Avrami-Erofeev reaction function, defined in (4), for the simulation of their pyrolysis.

3.3. Thermogravimetric analyses of the complete community masks under air

The mass and mass rate curves associated with the combustion of the five complete masks are gathered in Fig. 4.

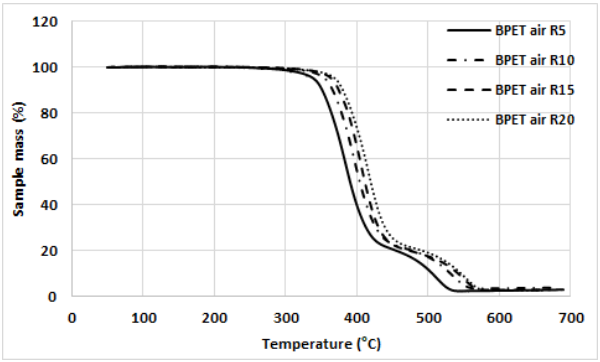
BPET air R5
BPET air R10
BPET air R15
BPET air R20
Sample mass (%)
Temperature (°C)

a)

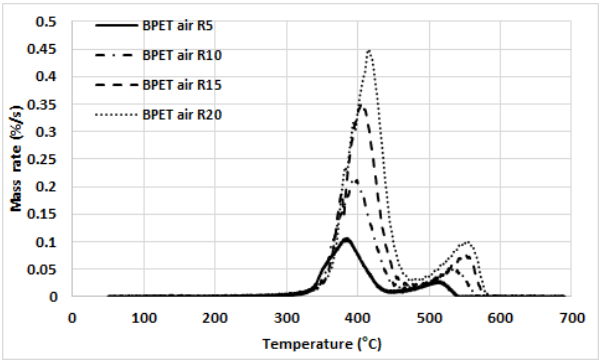
BPET air R5
BPET air R10
BPET air R15
BPET air R20
Mass rate (%/s)
Temperature (°C)

b)

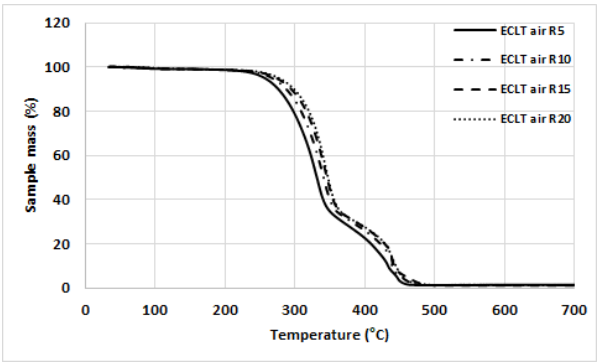
ECLT air R5
ECLT air R10
ECLT air R15
ECLT air R20
Sample mass (%)
Temperature (°C)

c)

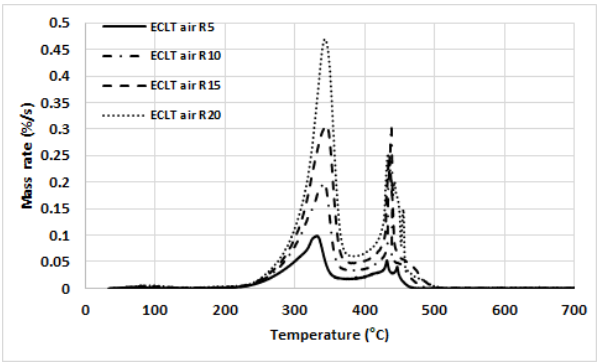
ECLT air R5
ECLT air R10
ECLT air R15
ECLT air R20
Mass rate (%/s)
Temperature (°C)

d)

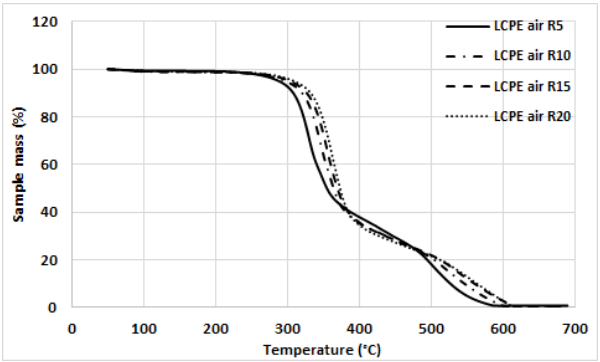
LCPE air R5
LCPE air R10
LCPE air R15
LCPE air R20
Sample mass (%)
Temperature (°C)

e)

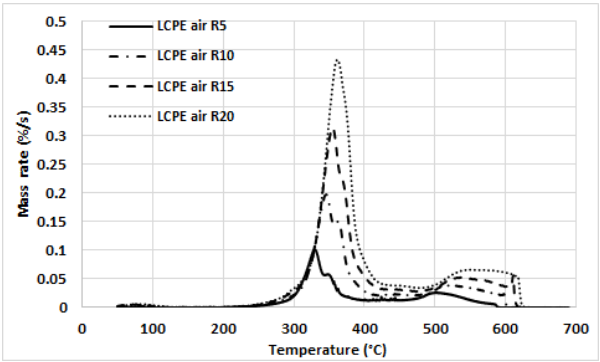
LCPE air R5
LCPE air R10
LCPE air R15
LCPE air R20
Mass rate (%/s)
Temperature (°C)

f)

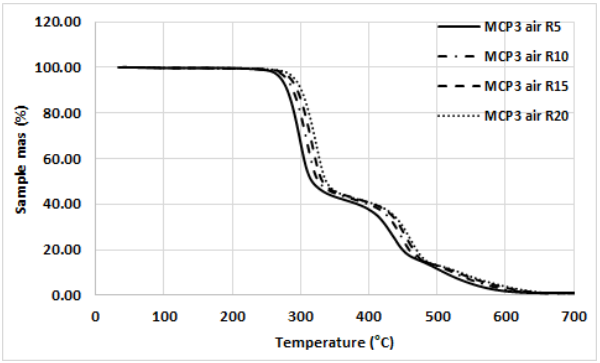
MCP3 air R5
MCP3 air R10
MCP3 air R15
MCP3 air R20
Sample mas (%)
Temperature (°C)

g)

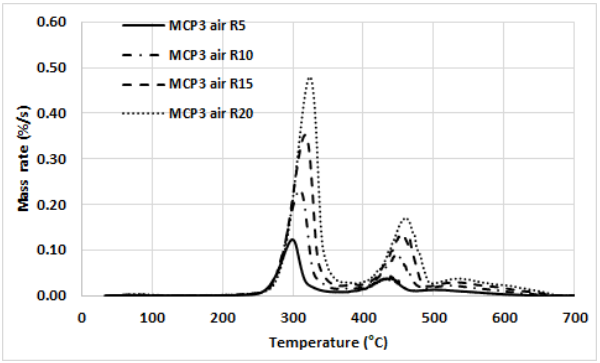
MCP3 air R5
MCP3 air R10
MCP3 air R15
MCP3 air R20
Mass rate (%/s)
Temperature (°C)

h)

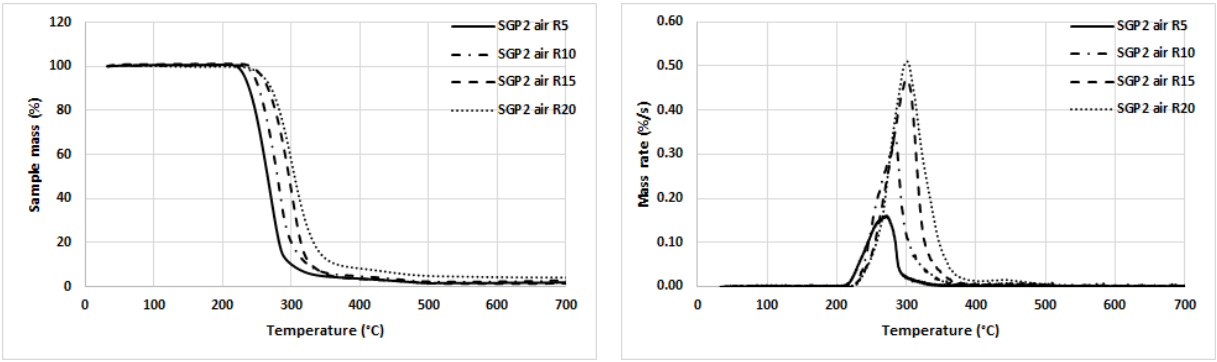

i) j)

459 **Fig. 4**. Mass curves for the combustion of the complete BPET a), ECLT c), LCPE e), MCP3 g), and SGP2
460 i) masks. Mass rate curves for the combustion of the complete BPET b), ECLT d), LCPE f), MCP3 h),
461 and SGP2 j) masks. In each figure, the curves corresponding to a temperature ramp of 5 °C/min (resp.
462 10, 15, 20) are represented with a solid line (resp. large hyphened, small hyphened, and dotted
463 lines).

464

465 Again, the shapes of the mass and mass rate curves look similar for each sample (these shapes do not
466 highly depend on the temperature ramp), but high differences occur from one sample to another
467 one:

468 - The mass rate curve of the BPET mask presents two peaks: a first large one between 390-415
469 °C and a second much smaller one between 501-554 °C. This mask is composed of two
470 synthetic fibers which are being degraded in slightly different temperature ranges.
471 - For the ECLT mask, the mass rate curves present two peaks. The second one is very thin and
472 looks like a needle. The first peak surely corresponds to the devolatilization stage, while the
473 second one corresponds to the combustion of the char structure. If this is the usual
474 combustion profile for lignocellulosic materials, the thinness of the second high peak may be
475 the consequence of the mixture of fibers.
476 - The LCPE mass rate curves present two peaks, the second one occurring during a quite wide
477 temperature interval ending after 600 °C.

- In the case of the MCP3 mask, two peaks can be identified and a long tail appears on the right-hand side of the second peak.
- The SGP2 mass rate curves present a unique peak followed by a small and quite long tail on its right-hand side. This mask only contains polypropylene.

The peaks move to higher temperatures when the temperature ramp increases, whatever the mask.

The characteristics (position and height) of each peak are gathered in Table 5, for the five masks.

Table 5. Position and height of each peak and final mass, for the combustion of the five complete masks.

Sample	First peak		Second peak		Final mass
	Temperature (°C)	Mass rate (%/s)	Temperature (°C)	Mass rate (%/s)	(%)
BPET					
R5	388.2	0.104	511.7	0.030	3.1
R10	395.4	0.215	539.4	0.049	4.0
R15	405.1	0.353	551.7	0.076	3.1
R20	415.4	0.449	548.9	0.100	2.9
ECLT					
R5	333.5	0.098	431.9	0.053	1.4
R10	341.8	0.198	438.3	0.305	1.2
R15	344.5	0.306	435.3	0.252	1.0
R20	343.2	1.484	433.7	0.254	1.2
LCPE					
R5	329.2	0.102	502.8	0.027	0.9
R10	346.3	0.198	520.7	0.040	0.6
R15	355.1	0.315	535.9	0.053	0.6
R20	361.6	0.433	547.4	0.067	0.1
MCP3					
R5	298.9	0.123	433.3	0.038	1.2
R10	309.7	0.237	448.3	0.087	0.9
R15	317.4	0.352	465.9	0.127	1.0
R20	324.2	0.479	463.2	0.168	1.0
SGP2					
R5	271.2	0.161	-	-	2.3
R10	282.9	0.337	-	-	3.2
R15	302.0	0.467	-	-	1.5
R20	301.6	0.510	-	-	3.9

The shifts of the peak position with respect to the temperature ramp lie between 15 and 33 °C, without clear tendency with respect to the composition of the mask. The first (devolatilization) peak occurs at lower temperatures under air than under pyrolysis: between 10 and 20 °C, depending on the mask. Oxygen is known to enhance the devolatilization process.

Again, the final mass does no obey a clear tendency with respect to the temperature ramp, whatever the mask.

The combustion of polyethylene terephthalate was performed in [30] under temperature ramps of 10, 20, 30, and 40 °C/min. The authors observed a main peak occurring between 420 and 500 °C, depending on the temperature ramp. A second peak was observed at approximately 600 °C. The observed combustion of the BPET mask is in good agreement with these results.

The combustion of cotton residue performed in [27] led to a devolatilization peak at approximately 320 °C and to a combustion of the char structure at 460 °C. The ECLT, LCPE and MCP3 masks, which contain cotton (and flax), present a quite similar combustion profile, even if some of them also contain synthetic fibers.

Combustion experiments were performed in [31]on polypropylene fibers and on blends with flax fibers, under a temperature ramp of 5 °C/min. The main mass losses were observed between 240 and 300 °C (the mass rate curves are not presented). Then the mass was slightly decreasing until 500 °C. The combustion of the SGP2 mask agrees with this result. The combustion of polypropylene was also studied in [32] under a temperature ramp of 10 °C/min. The main mass losses were observed between 280 and 350 °C.

3.4. Gaseous emissions during the combustion of the complete masks

The gaseous emissions (CO, CO_2, NO and THC) occurring during the combustion of the complete masks in the horizontal oven are presented in Fig. 5. These gaseous emissions are represented as ppm per gram of material to compare the results obtained for the five masks.

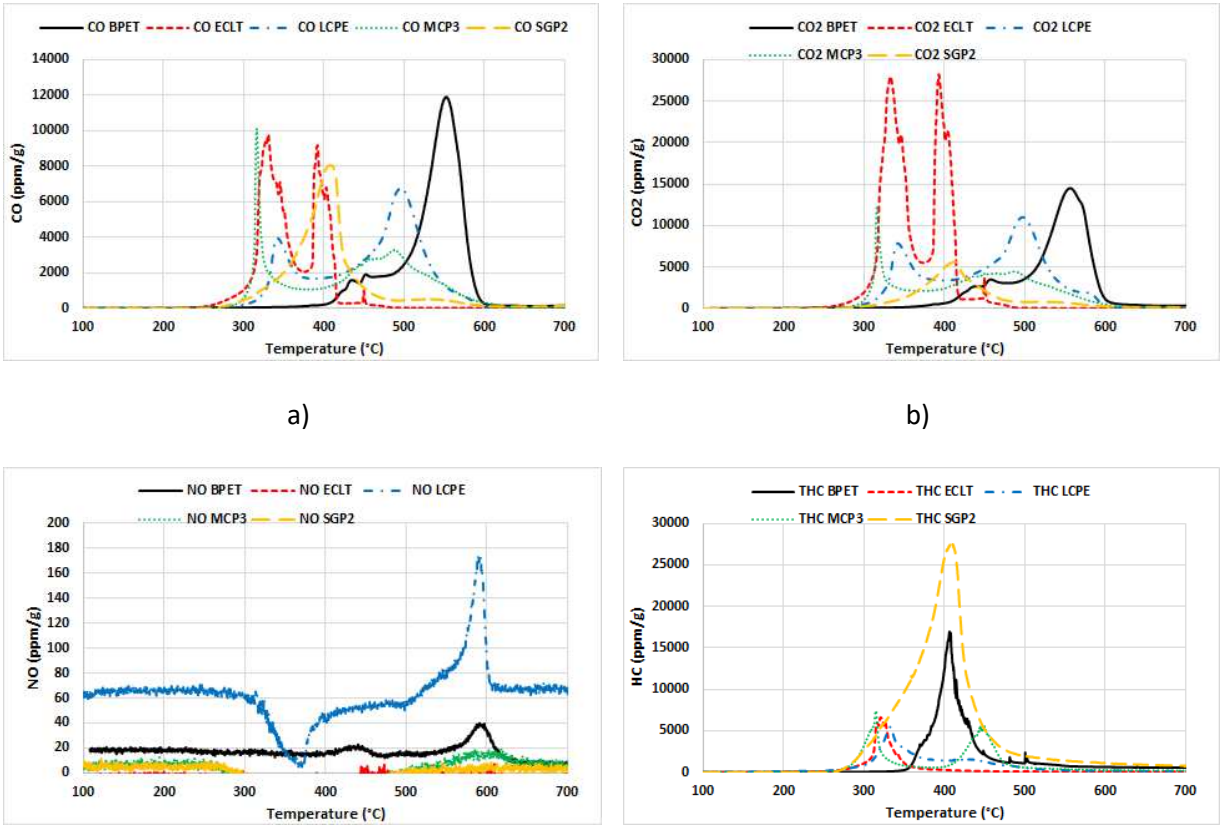

Fig. 5. Gaseous emissions: CO a), CO_2 b), NO c), and THC d), measured during a combustion test of the BPET (black, solid line), ECLT (red, small hyphened line), LCPE (blue, dotted -hyphened), MCP3 (green, dotted line), and SGP2 masks (yellow, large hyphened line), in a horizontal oven.

The NO_2 emissions are not presented, being lower than the detection limit, whatever the mask. The profiles of the gaseous emissions curves highly differ from one mask to another one. The amounts of NO are low, whatever the mask: at most 170 ppm/g to be compared to the other gaseous emissions which reach values higher than 12000 ppm/g. The low amount of nitrogen in each mask could explain these low NO emissions, see Table 3. For the SGP2 mask, the CO and CO_2 emissions present a

single peak. But the case of this mask will be discussed later on. For the BPET mask, the CO and CO_2 emissions present a single peak with an important shoulder on its left-hand side. This BPET mask presents the highest peak for the CO emissions. The CO and CO_2 emissions associated with the combustion of LCPE and of MCP3 mask present two peaks.

The position and the height of each peak of the gaseous (CO, CO_2 and THC) emissions are presented in Table 6, for the five complete masks.

Table 6. Characterizations of the peaks of the CO, CO_2 and THC emissions for the five complete masks.

Sample	Peak CO		Peak CO_2		Peak THC	
	Position (°C)	Height (ppm/g)	Position (°C)	Height (ppm/g)	Position (°C)	Height (ppm/g)
BPET	552.7	11892	555.9	14502	406.2	16961
ECLT						
Peak 1	330.7	9792	332.2	27989	320.5	6605
Peak 2	392.1	9177	393.0	28243	-	-
LCPE						
Peak 1	342.5	3948	342.1	7859	332.5	5484
Peak 2	494.9	6761	496.9	11020	-	-
MCP3						
Peak 1	316.5	10856	316.5	13312	314.3	7979
Peak 2	487.6	3519	487.6	4777	444.8	5875
SGP2	407.6	8053	412.4	5637	408.9	27600

The ECLT, LCPE and MCP3 masks contain cotton and present quite identical CO and CO_2 emission peaks in the temperature range 315-345 °C. The LCPE and MCP3 masks which also contain 30% polyamide present identical CO and CO_2 emission peaks at approximatively 500 °C. The BPET mask moreover contains polyester which seems to thermally decompose at higher temperatures (around 550 °C). The ECLT mask contains flax fibers, which can lead to the emission peaks occurring at approximately 330 °C. The SGP2 mask presents a unique emission peak at around 410 °C with uncertainties on the gaseous emission measurements to be discussed later on.

The CO emissions occurring during the combustion of polypropylene fibers were observed in [31] to present a unique peak occurring between 60 and 170 °C. When adding flax fibers to these

polypropylene fibers, the CO emissions were occurring in a much wider temperature range: 50-500 °C.

The gaseous emissions occurring during the combustion of polyethylene were analyzed in [33], using GC-FID and GC-MSD methods. The authors computed the yields of THC and polycyclic aromatic hydrocarbons (PAH) at the temperatures of 600, 700, 800, and 900 °C.

Gaseous emissions (mainly THC) were measured during the pyrolysis of a Korean surgical mask in [6]. They observed a unique peak in the temperature range 495-505 for CH_4, C_2H_6 and C_2H_4. When performing the slow pyrolysis of pure polyethylene terephthalate, the main component of the BPET mask, the authors found in [24] a maximal CO emission at 444 °C, much lower than the temperature at which the CO emissions reach their maximum for the BPET mask (551.7 °C).

Possible chemical reactions occurring during the pyrolysis of mask rope under helium are proposed in [10].

The overall amounts of gas emitted during the complete combustion process are computed by integration of the areas below the emissions curves presented in Fig. 5 and converted in moles per gram of material. They are presented in Fig 6.

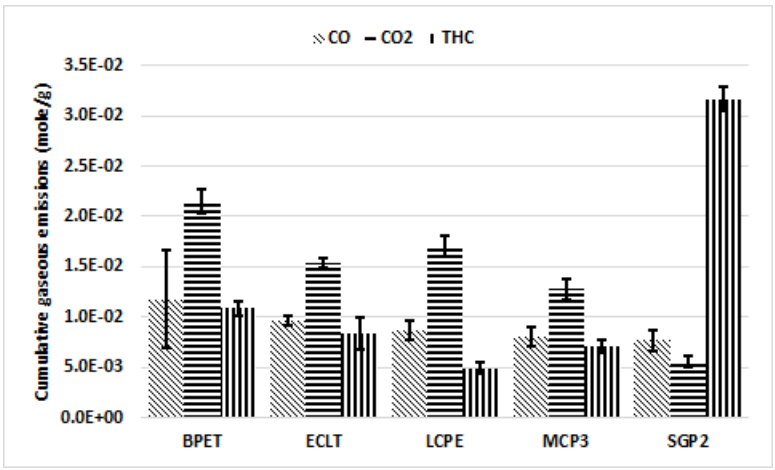

Fig. 6. Gaseous emissions (CO dashed, CO_2 horizontal lines, and THC vertical lines) for the five complete masks.

The five masks do not present very significant differences concerning the CO emissions: between $7.7x10^{-3}$ mol/g (for the SGP2 mask) and $1.2x10^{-2}$ mol/g (for the BPET mask). The SGP2 mask emits much lower CO_2 amounts (less than one half) than the other masks, but it emits much higher THC amounts (approximately three times higher) than the other masks. Its C fraction is the highest one among the five masks. The LCPE mask emits the lowest CO_2 emissions.

The amounts of NO and NO_2 are not reported in Fig. 6, being much lower than that of the other gases, whatever the mask and probably reaching the calibration limits, see Fig. 5 c) for the NO emissions.

The percentages of emitted carbon moles are gathered in Table 7 for the five complete masks.

Table 7. Evaluation of the carbon moles emitted during the combustion of each mask, and relative difference with the carbon amounts indicated in Table 2.

	BPET	**ECLT**	**LCPE**	**MCP3**	**SGP2**
Carbon emitted (%)	48.4	38.5	40.3	34.4	66.3
Rel. Diff. (%)	24	11	20	39	59

For the BPET, ECLT, LCPE, and MCP3 masks, the carbon content determined through the ultimate analyses of Table 3 and the carbon moles emitted during the combustion in the horizontal oven quite well agree. For the SGP2 mask, the relative difference is too high. The main reason is the limitation of the gas analyzer as described in section 2.3. This analyzer is indeed unable to detect chemical compounds with a number of carbon atoms greater than or equal to 10. In [34], the combustions of polypropylene, with 6.75% of syndiotactic fraction, and of polyethylene were performed under an isothermal temperature of 350 °C. The oxidation products were desorbed and conducted to a GC-MS device. Among the different chemical compounds found by the authors during the combustion

polypropylene, that with a number of C atoms greater than or equal to 10 have an area fraction greater than 48% of the total area of the chromatogram. This proves that at temperatures lower than 350 °C, significant emissions of THC are being emitted during the combustion of polypropylene and they are not detected by the gas analyzer which is used in the present study. Now considering the combustion polyethylene, the authors also found in [34] chemical compounds with a number of carbon atoms greater than or equal to 10. However, in this case, these compounds represent an area fraction lower than 25% of the total area of the chromatogram. This may explain the high relative differences observed in Table 7 for the BPET and MCP3 masks.

3.5. Determination of the optimal kinetic parameters for the pyrolysis of the complete masks

Simulations of the pyrolysis of the five complete masks were performed according to the procedure described in section 2.4.1. The number of constituents to be considered was determined in section 3.2. The optimal values of the kinetic parameters associated with the pyrolysis of the masks are gathered in Table 8.

Table 8. Fractions of constituents, optimal values of the kinetic parameters, and differences between the experimental and simulated mass and mass rate curves, for the pyrolysis of the five complete masks.

Sample	BPET	ECLT	LCPE	MCP3	SGP2
c_1	0.30	1.00	0.10	0.475	1.00
c_2	0.70		0.56	0.525	-
c_3	-		0.34	-	-
A_1 (1/s)	6.49×10^{14}	3.91×10^{12}	1.69×10^{12}	6.48×10^{14}	3.73×10^{15}
Ea_1 (J/mol)	210079.6	180074.0	162174.3	206079.6	249574.0
A_2 (1/s)	6.49×10^{14}	-	5.03×10^{14}	4.71×10^{8}	-
Ea_2 (J/mol)	220181.2	-	204074.0	149181.2	-
A_3 (1/s)	-	-	4.43×10^{8}	-	-
Ea_3 (J/mol)	-	-	145174.0	-	-

l_∞ (%)	Abs.	Rel.	Abs.	Rel.	Abs.	Rel.	Abs.	Rel.	Abs.	Rel.
R5	0.03	23.4%	0.03	15.8%	0.01	12.0%	0.02	19.6%	0.03	10.4%
R10	0.04	20.1%	0.05	13.2%	0.02	9.9%	0.02	9.4%	0.05	11.6%
R15	0.05	15.5%	0.07	11.3%	0.05	14.7%	0.04	13.4%	0.05	6.5%
R20	0.08	16.0%	0.08	10.6%	0.10	24.6%	0.06	15.9%	0.08	8.9%
l_2 (%/s)										
R5	0.10		0.11		0.05		0.07		0.06	
R10	0.17		0.21		0.14		0.08		0.13	
R15	0.26		0.24		0.28		0.19		0.12	
R20	0.40		0.35		0.42		0.32		0.22	
R_m^2										
R5	1.00		1.00		1.00		1.00		1.00	
R10	1.00		1.00		1.00		1.00		1.00	
R15	1.00		1.00		1.00		1.00		1.00	
R20	1.00		1.00		1.00		1.00		1.00	
R_{mr}^2										
R5	0.97		0.98		0.98		0.98		0.99	
R10	0.97		0.98		0.98		0.99		0.99	
R15	0.98		0.98		0.96		0.98		0.99	
R20	0.97		0.98		0.94		0.97		0.99	
R_o^2										
R5	0.96		0.97		0.98		0.97		0.99	
R10	0.96		0.97		0.98		0.99		0.99	
R15	0.97		0.98		0.96		0.98		0.99	
R20	0.96		0.98		0.93		0.97		0.99	

Mampel's reaction function was chosen for all masks and constituents, except for ECLT and SGP2 masks, for which the second-order Avrami-Erofeev reaction function was chosen for the unique constituent of these masks, because of the thinness of the unique devolatilization peak.

The R_m^2 determination coefficients for the mass are equal to 1 whatever the mask and temperature ramp. The R_{mr}^2 determination coefficients for the mass rate lies between 0.94 and 0.99 and the overall determination coefficient R_o^2 lies between 0.93 and 0.99. All these determination coefficients are sufficiently close to 1 to accept the simulations with the indicated numbers of constituents and the optimal values of the pre-exponential and activation energies indicated in Table 8 and determined through the procedure described in section 2.4.1.

Activation energies between 180 and 234 kJ/mol were found in [25] for the pyrolysis of polyamide, depending on the extent of conversion and on the chosen model-free or model-based method. The

608 corresponding pre-exponential factors were found in the range 5.25×10^{11} and 1.88×10^{22} 1/s, which
609 represent very high values. The reason is the presence of a thin and high peak. An activation energy
610 of 180±10 kJ/mol and a pre-exponential factor equal to exp(10.6) 1/s were found in [35] for the
611 pyrolysis of polyamide 6. The authors here used the Coats-Redfern method.

612 For the combustion of cotton and using a fourth-order Avrami-Erofeev reaction, an energy activation
613 of 205.3 kJ/mol and a pre-exponential factor of to 3.5×10^{14} 1/s were found in [27]. Other reaction
614 functions were here tested.

615 Applying in [28] an isoconversional method to determine the kinetic parameters associated with the
616 pyrolysis of pure polypropylene, the authors found activation energies lying in the range 161-173
617 kJ/mol, when considering a reaction order equal to 1. The pre-exponential factors were found in the
618 range 4.97×10^{9}-4.97×10^{10} 1/s. In [21], the authors applied a Coats-Redfern method to determine the
619 kinetic parameters associated with the pyrolysis of polypropylene and they obtained an activation
620 energy equal to 219073.9 J/mol and a pre-exponential factor equal to 4.349×10^{13} 1/s.

621 Differences between the values of the kinetic parameters indicated in Table 8 and the literature may
622 be explained by the choices of the kinetic models or methods but also by differences on the materials
623 which are considered. As already indicated, the fibers which are used for the fabrication of the
624 community masks may be mixed or treated.

625

626 *3.6. Determination of the optimal kinetic parameters for the combustion of the complete masks*

627 Simulations of the combustion of the five masks were performed according to the procedure
628 described in section 2.4.2 completed with the Supplementary Material.

629 The number of constituents to be considered in the combustion of the community masks was taken
630 equal to that of the pyrolysis process. The first-order reaction function: $f_1(\alpha) = 1 - \alpha$ was chosen
631 for most masks and constituents. Because of the thinness of the peaks observed in Fig. 4, an Avrami-

Erofeev reaction function of order 4 was chosen for the combustion of the unique component of the ECLT mask, and an Avrami-Erofeev reaction function of order 2 was chosen for the combustion of the unique component of the SGP2 mask.

The optimal values of the kinetic parameters associated with the combustion of the masks are gathered in Table 9.

Table 9. Fractions of constituents, proportion of volatiles in these constituents, optimal values of the kinetic parameters, and differences between the experimental and simulated mass and mass rate curves, for the combustion of the five complete masks.

Sample	**BPET**		**ECLT**		**LCPE**		**MCP3**		**SGP2**	
c_1	0.3		1.00		0.10		0.70		1.00	
c_2	0.7		-		0.59		0.30		-	
c_3	-		-		0.31		-		-	
$\tau_{vol,1}$	0.70		0.80		0.90		0.85		0.98	
$\tau_{vol,2}$	0.85		-		0.85		0.90		-	
$\tau_{vol,3}$	-		-		0.60		-		-	
A_1 (1/s)	5.42×10^{14}		1.69×10^{9}		5.70×10^{12}		2.52×10^{13}		6.09×10^{5}	
Ea_1 (J/mol)	213322.1		133874.2		170000.0		172122.0		88173.8	
A_2 (1/s)	2.42×10^{13}		-		9.63×10^{13}		2.42×10^{13}		-	
Ea_2 (J/mol)	202522.1		-		192000.0		212522.1		-	
A_3 (1/s)	-		-		2.99×10^{3}		-		-	
Ea_3 (J/mol)	-		-		81500.0		-		-	
A_{comb} (1/s)	9.70×10^{7}		1.50×10^{10}		7.24×10^{3}		9.72×10^{3}		1.50×10^{5}	
Ea_{comb} (J/mol)	221100.0		226000.0		165000.0		161100.0		153000.0	
l_∞ (%)	Abs.	Rel.	Abs.	Rel.	Abs.	Rel.	Abs.	Rel.	Abs.	Rel.
R5	0.03	24.7%	0.03	30.3%	0.05	44.9%	0.02	12.6%	0.04	25.1%
R10	0.04	18.0%	0.13	57.2%	0.05	22.5%	0.03	11.1%	0.12	34.9%
R15	0.04	12.6%	0.13	47.4%	0.06	17.4%	0.04	10.1%	0.05	10.7%
R20	0.05	11.5%	0.17	34.8%	0.08	18.5%	0.10	21.2%	0.08	20.8%
l_2 (%/s)										
R5	0.10		0.14		0.15		0.09		0.11	
R10	0.16		0.26		0.21		0.15		0.40	
R15	0.24		0.38		0.30		0.23		0.22	
R20	0.26		0.68		0.45		0.42		0.31	
R_m^2										
R5	1.00		1.00		0.99		1.00		1.00	
R10	1.00		1.00		1.00		1.00		1.00	
R15	1.00		1.00		1.00		1.00		1.00	

R20	1.00	1.00	1.00	1.00	1.00
R_{mr}^2					
R5	0.97	0.88	0.84	0.95	0.97
R10	0.98	0.91	0.93	0.97	0.89
R15	0.98	0.91	0.95	0.97	0.98
R20	0.98	0.85	0.94	0.94	0.96
R_o^2					
R5	0.96	0.88	0.84	0.95	0.97
R10	0.97	0.90	0.93	0.96	0.88
R15	0.98	0.91	0.94	0.96	0.98
R20	0.98	0.85	0.94	0.94	0.96

The R_m^2 determination coefficients for the mass is always greater than 0.99, which proves that the present simulations well represent the evolution of the mass, along the combustion process, whatever the temperature ramp and mask. The R_{mr}^2 determination coefficients for the mass rate takes quite low values for the ECLT mask, under the temperature ramps of 5 and 20 °C/min, for the MCP3 mask, under the temperature ramp of 5 °C/min, and for the SGP2 mask, under the temperature ramp of 10 °C/min. This means that the thin peaks are not well reproduced through these simulations. As the optimization procedure is simultaneously performed on the four temperature ramps, heat transfers could be more important in samples containing a mixture of natural and synthetic fibers. Such further heat transfers are not taken into account in the model, see for example [27] for an example where such heat transfers are taken into account in the case of cotton.

For the combustion of polyamide 6 and using the Coats-Redfern method, the authors found in [35] an activation energy of 250±20 kJ/mol and a pre-exponential factor equal to exp(16.3) 1/s.

For the combustion of cotton and using a fourth-order Avrami-Erofeev reaction, the authors found in [27] an energy activation of 128.3 kJ/mol and a pre-exponential factor of to 5.4×10^{15} 1/s.

A kinetic modeling of the combustion of polypropylene was performed in [32]. The reaction function $f(\alpha) = (1-\alpha)^n$ is considered. The combustion was decomposed in three stages. In the main stage, the authors took a reaction order *n* equal to 0.5 and found an activation energy equal to 230 kJ/mol

659 and a pre-exponential factor equal to 2.0×10^{14} 1/s. The kinetic parameters found for the combustion
660 of the SGP2 mask are in good agreement with these values.

661 Again the differences between the values gathered in Table 9 and that of the literature may be
662 explained by the choice of the kinetic models or methods.

663

664 *3.7. Examples of simulations of pyrolysis or combustion of the complete masks*

665 *3.7.1. Pyrolysis case*

666 As already indicated, the values of the determination coefficients are very close to 1 whatever the
667 mask and temperature ramp. The values of the determination coefficient R^2_{mr} lie between 0.94 for
668 the LCPE mask and 0.99 for the SGP2 mask. The cases of the ECLT mask under the temperature ramp
669 of 15 °C/min and LCPE mask under the temperature ramp of 20 °C/min will be considered. Fig. 7
670 gathers the experimental and simulated mass and mass rate curves for these two examples.

671

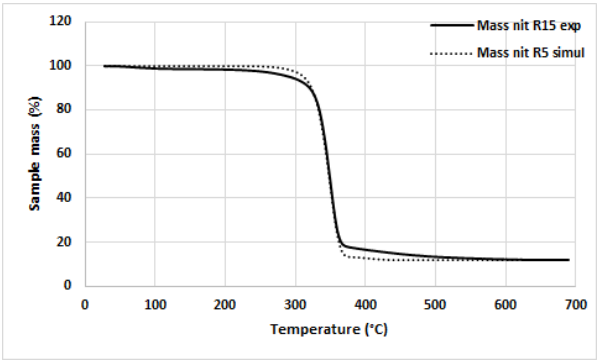

a)

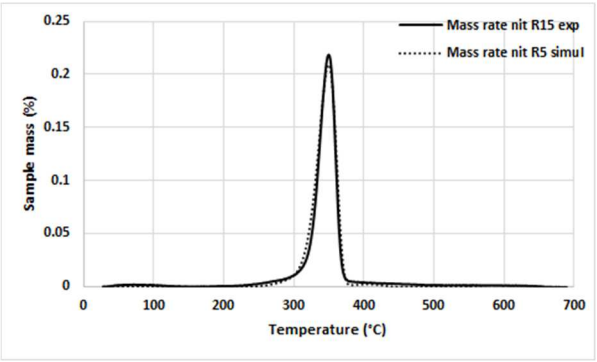

b)

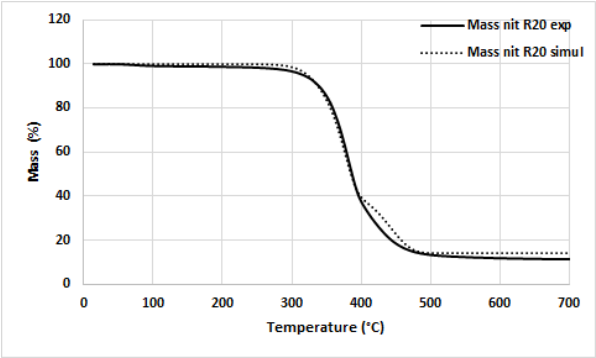

c)

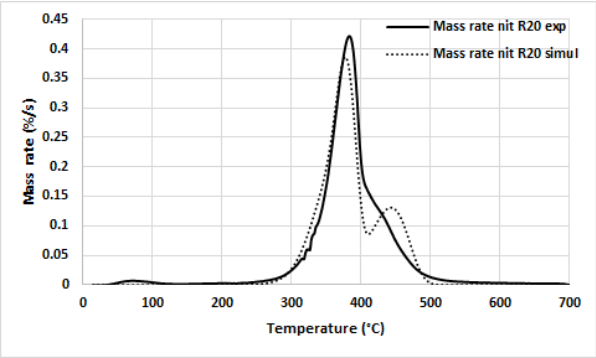

d)

672 **Fig. 7**. Experimental (solid line) and simulated (dotted line) mass a) and mass rate b) curves for the
673 pyrolysis of the ECLT mask under the temperature ramp of 15 °C/min. Experimental (solid line) and
674 simulated (dotted line) mass c) and mass rate d) curves for the pyrolysis of the LCPE mask under the
675 temperature ramp of 20 °C/min.

676

677 For the ECLT mask, the simulation very slightly overestimates the degradation between 200 and 300 °C and
678 underestimates this degradation between 350 and 500 °C. A further constituent could be considered, whose
679 degradation occurs between 200 and 300 °C. Nevertheless, its proportion should be very small. For the LCPE
680 mask, the moisture evaporation was not simulated in the present model. The simulated mass rate curve
681 struggles to reach the top of the experimental peak. The shoulder on the right-hand side of the peak is replaced
682 in the simulated mass rate curve by a second peak, see the previous discussion on the transformation of peaks
683 to shoulders depending on the temperature ramp. The optimization process performed on the four
684 temperature ramps simultaneously may certainly explain these differences between experimental and
685 simulated mass and mass rate curves. Nevertheless, the maximal difference between the experimental and
686 simulated mass and mass rate curves are here low and the R^2_{mr} and R^2_o are sufficiently close to 1 so that the
687 simulations may be accepted.
688 Similar situations occur for the other temperature ramps and for the other masks (not presented
689 here).

690

691 *3.7.2. Combustion case*

692 For the combustion of the five community masks, the determination coefficient R_m^2 lies between
693 0.99 and 1.00. The determination coefficient R_{mr}^2 lies between 0.85 for the ECLT mask under a
694 temperature ramp of 20 °C/min and 0.98 for other masks.

695 Simulations of combustion processes performed in the thermobalance are gathered in Fig. 8.

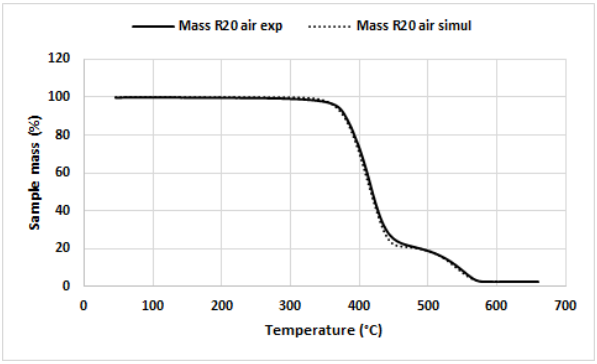

a)

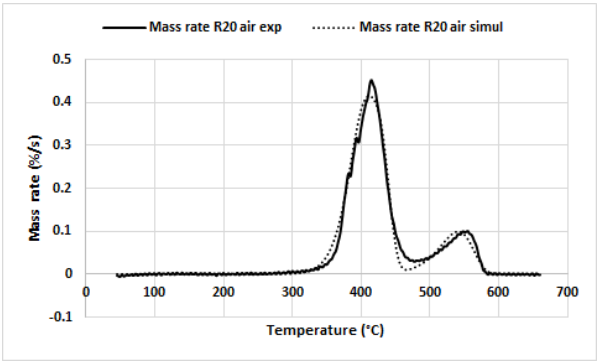

b)

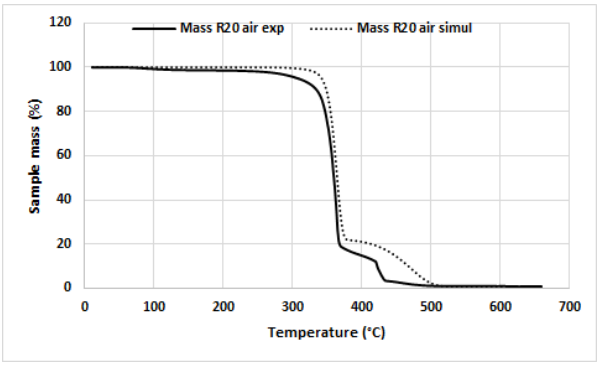

c)

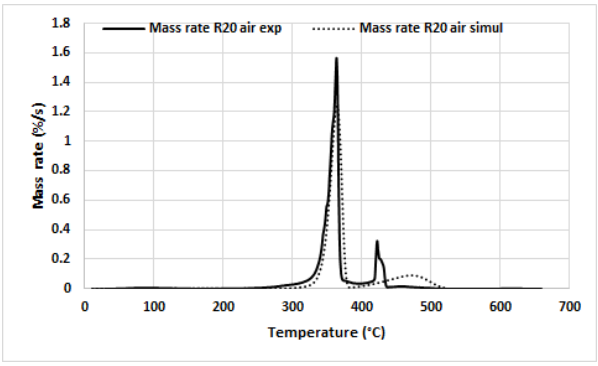

d)

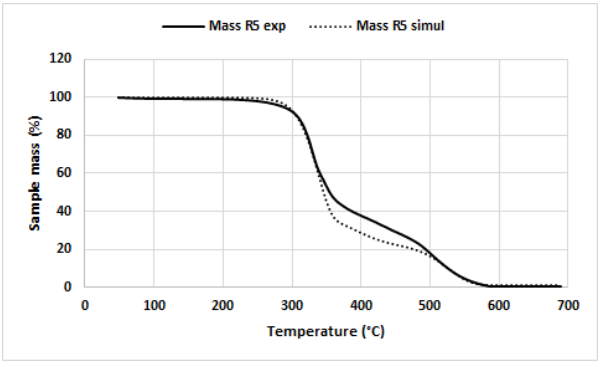

e)

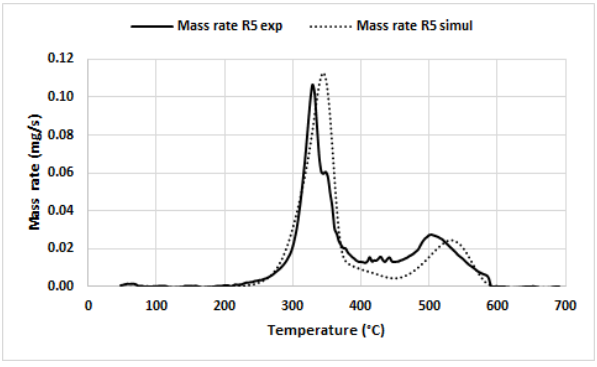

f)

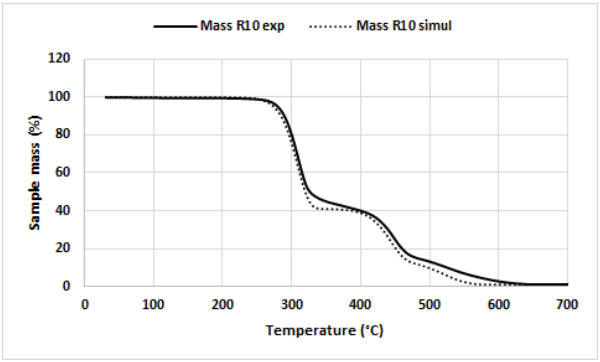

g)

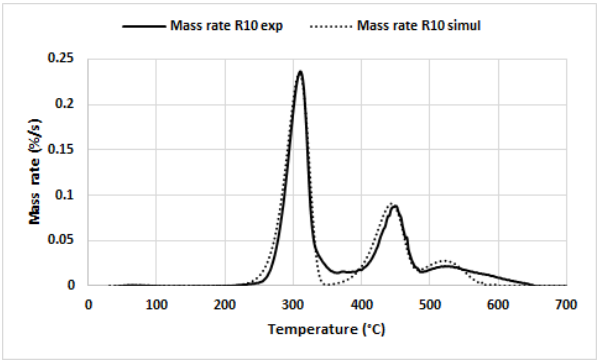

h)

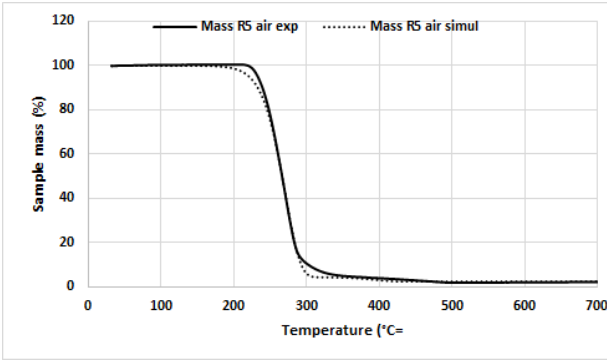

i)

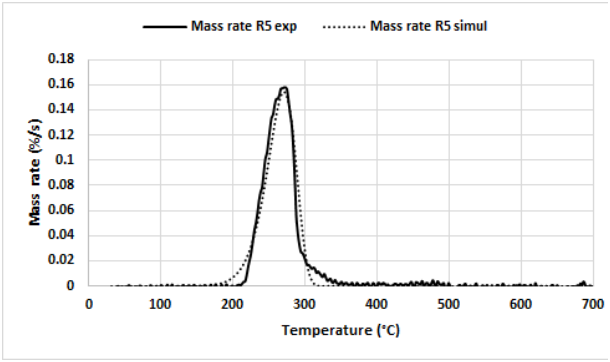

j)

Fig. 8. Experimental (solid line) and simulated (dotted line) mass and mass rate curves for BPET mask under a temperature ramp of 20 °C/min a) and b), ECLT mask under a temperature ramp of 20 °C/min c) and d), LCPE mask under a temperature ramp of 5 °C/min e) and f), MCP3 mask under a temperature ramp of 10 °C/min g) and h), and SGP2 mask under a temperature ramp of 5 °C/min, i) and j).

As proved in Table 8 through the different measures of the difference between the experimental and simulated mass rate curves prove that the mass curves and the shape of the mass rate curves are quite well simulated, whatever the mask and the temperature ramp, even if in the case of ECLT mask, the needle of the second peak is replaced by a quite flat peak, Fig. 8 d).

3.8. Comparisons between the mass rate and gaseous emissions curves

It is possible to superimpose the mass rate curves corresponding to combustion processes performed in the thermobalance under the temperature ramp of 5 °C/min and the gaseous emissions measured along combustion processes performed in the horizontal oven under the temperature ramp of approximately 5.5 °C/min.

The mass rate and emissions peaks do not always perfectly superimpose as shown in Fig. 9.

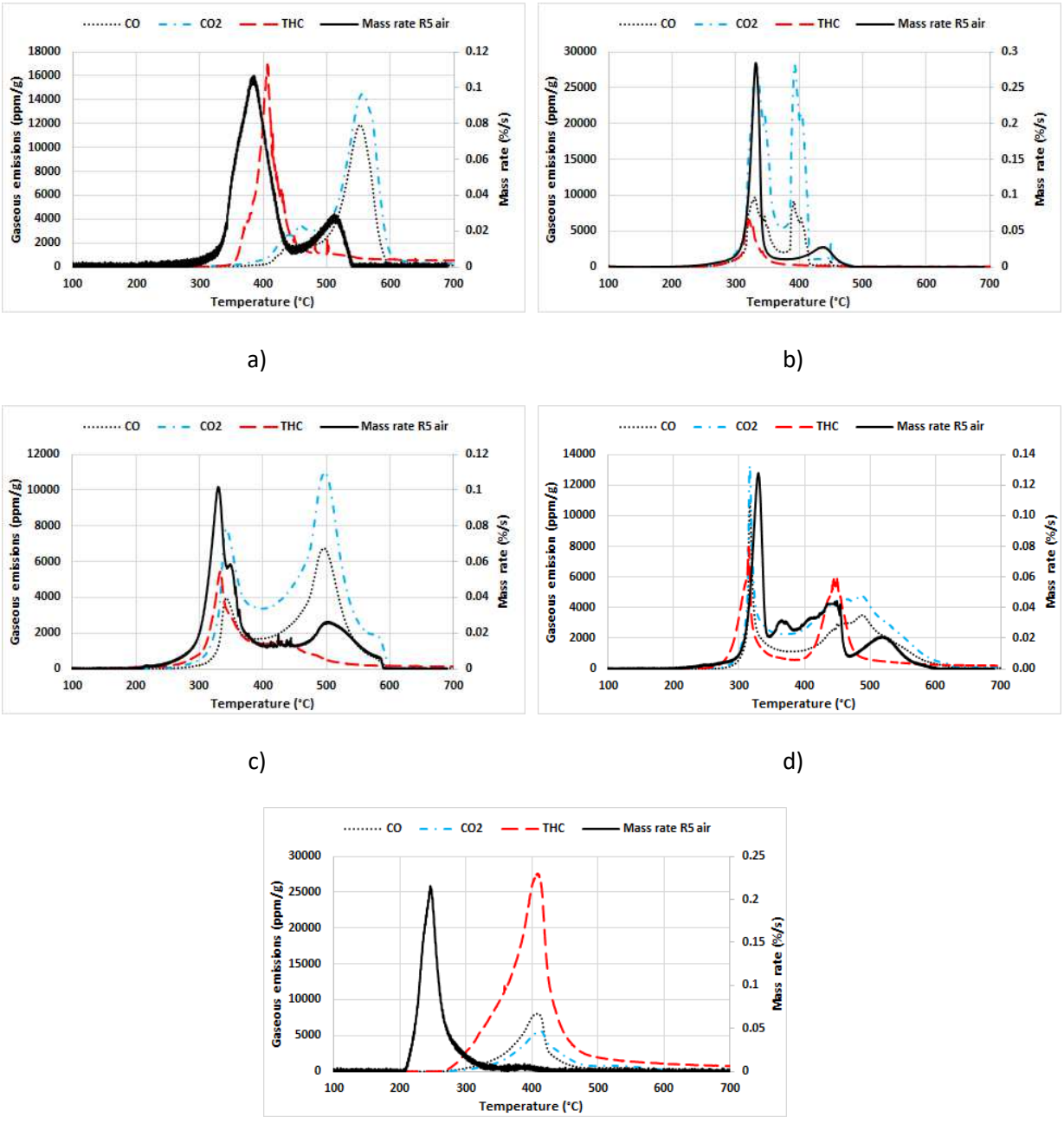

713 **Fig. 9**. Mass rate (solid line, secondary axis) and gaseous emissions (CO, black dotted line, CO2, blue,
714 hyphens-dots, THC, red large hyphens, primary axis) curves for BPET a) and ECLT b), LCPE c), MCP3 d),
715 and SGP2 e) masks.

716

717 For the BPET mask a), the CO emission peak appears at much higher temperatures than the
718 devolatilization and combustion peaks. For this ECLT mask, and also for the LCPE and MCP3 masks,
719 the first CO emissions peak occurs exactly in the same temperature range as the combustion peak.
720 The second peak appears earlier and is much thinner than the small second combustion peak.

721 Quite similar observations can be indicated for the CO_2 and THC emissions peaks.

722 For the SGP2 mask, the observed gaseous emissions occur at much higher temperatures than the
723 devolatilization peak. This may be due to the limitation of the analyzer used in these combustion
724 experiments. As already indicated, the analyzer is unable to detect chemical compounds with a
725 number of carbon atoms greater than or equal to 10. As indicated in section 3.4, 48% of the
726 emissions occur from the combustion of a polypropylene sample at temperatures lower than 350 °C,
727 with a number of carbon atoms greater than 10. This means that a peak of emitted gases surely
728 occur between 200 and 350 °C which is not detected by the analyzer used in the present study, see
729 the Supplementary Material for a simulation of these gaseous emissions in the SGP2 case.

730 For the NO and NO_2 emissions which are not presented in Fig. 9, the comparison between the mass
731 rate and gaseous emissions curves is more complicated as the levels of these gaseous emissions are
732 quite low and may be affected by calibration limits.

733

734 ## 4. Conclusion

735 Because of the Covid-19 pandemic, citizens are encouraged, if not forced, to wear community masks.
736 In the present study, pyrolysis and combustion experiments were performed on five community

737 masks presenting different compositions (natural or synthetic fibers), under low temperature ramps
738 of 5, 10, 15, and 20 °C/min. The main gaseous emissions were continuously measured during
739 combustion experiments performed under a temperature ramp approximately equal to 5 °C/min. A
740 kinetic modeling of these pyrolysis and combustion experiments was realized through the EIPR
741 model, the number of constituents to be considered being deduced from the mass and mass rate
742 curves of the pyrolysis case. The optimal values of the activation energies associated with the
743 pyrolysis of the masks were found equal to 210-220, 180, 145-209, 149-206 and 250 kJ/mol for the
744 pyrolysis of the BPET, ECLT, LCPE, MCP3 and SGP2 masks, depending on their constituents. For the
745 combustion of these masks, the activation energies were found equal to 202-213, 134, 82-192, 172-
746 213 and 88 kJ/mol. The activation energy associated with the combustion of the char was found
747 between 153 and 226 kJ/mol depending on the mask. These values are quite in good agreement with
748 that of the literature for the fibers of these masks. The eventual small differences which are observed
749 may be the consequence of either a mixture of different fibers or of a treatment applied to these
750 fibers before the fabrication of the masks. The gaseous emissions were observed in good agreement
751 with the combustion of the masks, except for the SGP2 mask totally composed of polypropylene
752 fibers. A large amount of gaseous emissions was missing certainly with a number of carbon atoms
753 greater than 10 as such chemical compounds cannot be detected by the gas analyzer which was used
754 in the present study. These missing gaseous emissions lie in the temperature range 200-350 °C.
755 The thermal degradations of such masks could be considered for energy production, the components
756 being involved in the fabrication of these masks being also present in other domestic waste. The
757 ECLT mask could be treated as a textile waste, being totally composed of cellulosic fibers. For the
758 four other masks, it is illusory to treat separately the different layers of the other masks. The
759 combustion of such complex masks could be considered for energy production, as soon as the usual
760 depollution systems against pollutant gaseous emissions are disposed. Performing thermal
761 degradations of such community masks in a drop tube furnace would help simulating the behavior of
762 such waste in industrial boilers.

References

[1] EU. Regulation (EU) 2017/745 of the European Parliament and of the Council of 5 April 2017 on medical devices 2017.

[2] Aragaw TA. Surgical face masks as a potential source for microplastic pollution in the COVID-19 scenario. Marine Pollution Bulletin 2020;159:111517. https://doi.org/10.1016/j.marpolbul.2020.111517.

[3] De-la-Torre GE, Rakib MdRJ, Pizarro-Ortega CI, Dioses-Salinas DC. Occurrence of personal protective equipment (PPE) associated with the COVID-19 pandemic along the coast of Lima, Peru. Science of The Total Environment 2021;774:145774. https://doi.org/10.1016/j.scitotenv.2021.145774.

[4] Selvaranjan K, Navaratnam S, Rajeev P, Ravintherakumaran N. Environmental challenges induced by extensive use of face masks during COVID-19: A review and potential solutions. Environmental Challenges 2021;3:100039. https://doi.org/10.1016/j.envc.2021.100039.

[5] Saberian M, Li J, Kilmartin-Lynch S, Boroujeni M. Repurposing of COVID-19 single-use face masks for pavements base/subbase. Science of The Total Environment 2021;769:145527. https://doi.org/10.1016/j.scitotenv.2021.145527.

[6] Jung S, Lee S, Dou X, Kwon EE. Valorization of disposable COVID-19 mask through the thermo-chemical process. Chemical Engineering Journal 2021;405:126658. https://doi.org/10.1016/j.cej.2020.126658.

[7] Chew KW, Chia SR, Chia WY, Cheah WY, Munawaroh HSH, Ong W-J. Abatement of hazardous materials and biomass waste via pyrolysis and co-pyrolysis for environmental sustainability and circular economy. Environmental Pollution 2021;278:116836. https://doi.org/10.1016/j.envpol.2021.116836.

[8] Purnomo CW, Kurniawan W, Aziz M. Technological review on thermochemical conversion of COVID-19-related medical wastes. Resources, Conservation and Recycling 2021;167:105429. https://doi.org/10.1016/j.resconrec.2021.105429.

[9] Su G, Ong HC, Ibrahim S, Fattah IMR, Mofijur M, Chong CT. Valorisation of medical waste through pyrolysis for a cleaner environment: Progress and challenges. Environmental Pollution 2021;279:116934. https://doi.org/10.1016/j.envpol.2021.116934.

[10] Chen R, Zhang D, Xu X, Yuan Y. Pyrolysis characteristics, kinetics, thermodynamics and volatile products of waste medical surgical mask rope by thermogravimetry and online thermogravimetry-Fourier transform infrared-mass spectrometry analysis. Fuel 2021;295:120632. https://doi.org/10.1016/j.fuel.2021.120632.

[11] Amutio M, Lopez G, Aguado R, Artetxe M, Bilbao J, Olazar M. Kinetic study of lignocellulosic biomass oxidative pyrolysis. Fuel 2012;95:305–11. https://doi.org/10.1016/j.fuel.2011.10.008.

[12] Norme AFNOR SPEC 76-001 n.d.

[13] Afnor. Medical face masks - Requirements and test methods. NF EN 14683+AC August 2019 2019.

[14] Afnor. Textiles. Determination of permeability of fabrics to air. NF EN ISO 9237 August 1995 1995.

[15] ISO 1171:2010 Solid mineral fuels — Determination of ash n.d.

[16] Afnor. Solid biofuels - Determination of ash content - Biocarburants solides. NF EN ISO 18122 Décembre 2015 2015.

[17] Afnor. Solid mineral fuels - Determination of total carbon, hydrogen and nitrogen content - Instrumental method. ISO 29541:2010 October 2010 2010.

[18] Afnor. Solid mineral fuels - Determination of sulfur by IR spectroscopy. ISO 19579:2006 October 2006 2006.

[19] D05 Committee. Practice for Ultimate Analysis of Coal and Coke. ASTM D3176 - 15. ASTM International; n.d. https://doi.org/10.1520/D3176-15.
[20] Van Krevelen DW, Te Nijenhuis K. Properties of Polymers Their Correlation with Chemical Structure ; their Numerical Estimation and Prediction from Additive Group Contributions. Amsterdam, Nederlands: Elsevier Science & Technology Books; 2009.
[21] Janajreh I, Adeyemi I, Elagroudy S. Gasification feasibility of polyethylene, polypropylene, polystyrene waste and their mixture: Experimental studies and modeling. Sustainable Energy Technologies and Assessments 2020;39:100684. https://doi.org/10.1016/j.seta.2020.100684.
[22] Park K-B, Jeong Y-S, Kim J-S. Activator-assisted pyrolysis of polypropylene. Applied Energy 2019;253:113558. https://doi.org/10.1016/j.apenergy.2019.113558.
[23] Parku GK, Collard F-X, Görgens JF. Pyrolysis of waste polypropylene plastics for energy recovery: Influence of heating rate and vacuum conditions on composition of fuel product. Fuel Processing Technology 2020;209:106522. https://doi.org/10.1016/j.fuproc.2020.106522.
[24] Dhahak A, Hild G, Rouaud M, Mauviel G, Burkle-Vitzthum V. Slow pyrolysis of polyethylene terephthalate: Online monitoring of gas production and quantitative analysis of waxy products. Journal of Analytical and Applied Pyrolysis 2019;142:104664. https://doi.org/10.1016/j.jaap.2019.104664.
[25] Pannase AM, Singh RK, Ruj B, Gupta P. Decomposition of polyamide via slow pyrolysis: Effect of heating rate and operating temperature on product yield and composition. Journal of Analytical and Applied Pyrolysis 2020;151:104886. https://doi.org/10.1016/j.jaap.2020.104886.
[26] Herrera M, Matuschek G, Kettrup A. Thermal degradation studies of some aliphatic polyamides using hyphenated techniques (TG-MS, TG-FTIR). Journal of Thermal Analysis and Calorimetry 2000;59:385–94. https://doi.org/10.1023/A:1010177105297.
[27] Brillard A, Habermacher D, Brilhac J-F. Thermal degradations of used cotton fabrics and of cellulose: kinetic and heat transfer modeling. Cellulose 2017;24:1579–95. https://doi.org/10.1007/s10570-017-1200-6.
[28] Gao Z, Kaneko T, Amasaki I, Nakada M. A kinetic study of thermal degradation of polypropylene. Polymer Degradation and Stability 2003;80:269–74. https://doi.org/10.1016/S0141-3910(02)00407-X.
[29] Hujuri U, Ghoshal AK, Gumma S. Modeling pyrolysis kinetics of plastic mixtures. Polymer Degradation and Stability 2008;93:1832–7. https://doi.org/10.1016/j.polymdegradstab.2008.07.006.
[30] Oh S-C, Lee D-G, Kwak H, Bae S-Y. Combustion kinetics of polyethylene terephtalate. Environmental Engineering Research 2006;11:250–6. https://doi.org/10.4491/eer.2006.11.5.250.
[31] Le Bras M, Duquesne S, Fois M, Grisel M, Poutch F. Intumescent polypropylene/flax blends: a preliminary study. Polymer Degradation and Stability 2005;88:80–4. https://doi.org/10.1016/j.polymdegradstab.2004.04.028.
[32] Vovelle C, Mellottée H. Étude de la cinétique de la dégradation thermique du polypropylène et du polystyrène par analyse thermogravimétrique. European Polymer Journal 1983;19:387–90. https://doi.org/10.1016/0014-3057(83)90111-8.
[33] Piao M, Chu S, Zheng M, Xu X. Characterization of the combustion products of polyethylene. Chemosphere 1999;39:1497–512. https://doi.org/10.1016/S0045-6535(99)00054-5.
[34] Mitera J, Michal J, Kubat J, Kubelka V. Analysis of thermo-oxidation products of polypropylene and polyethylene by Gas chromatography/mass spectrometry. Z Anal Chem 1976;281:23–7. https://doi.org/10.1007/BF01155812.
[35] Dabrowski F, Bourbigot S, Delobel R, Le Bras M. Kinetic modelling of the thermal degradation: of polyamide-6 nanocomposite. European Polymer Journal 2000;36:273–84. https://doi.org/10.1016/S0014-3057(99)00079-8.

Community mask

Thermogravimetric analyses
5,10,15,20 °C/min

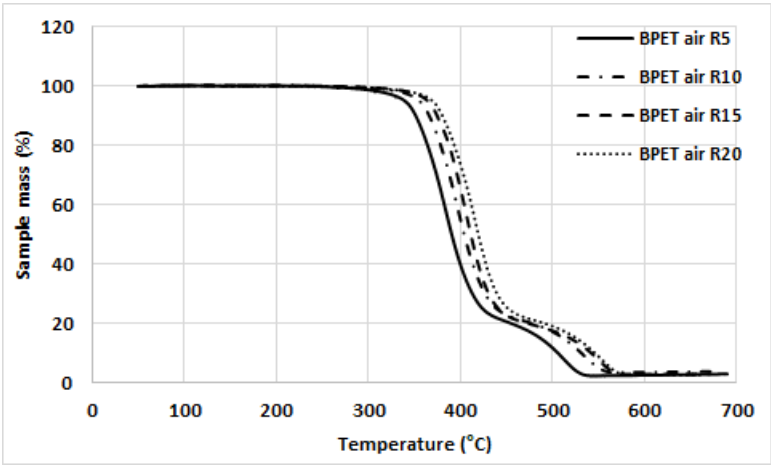

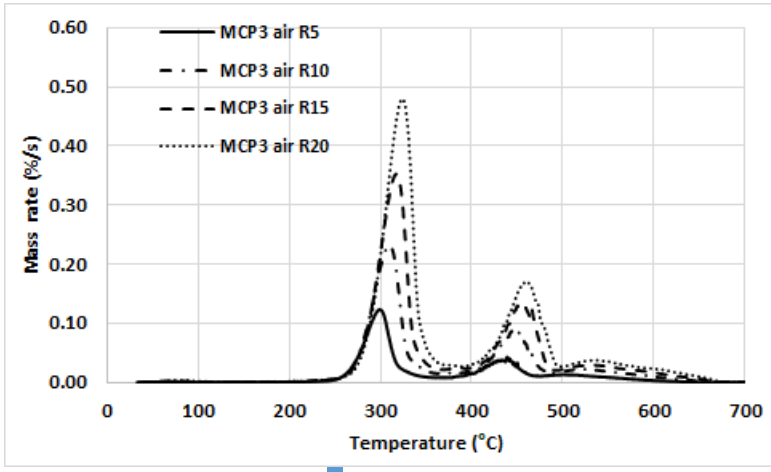

Gaseous emisssions
during combustion
5 °C/min

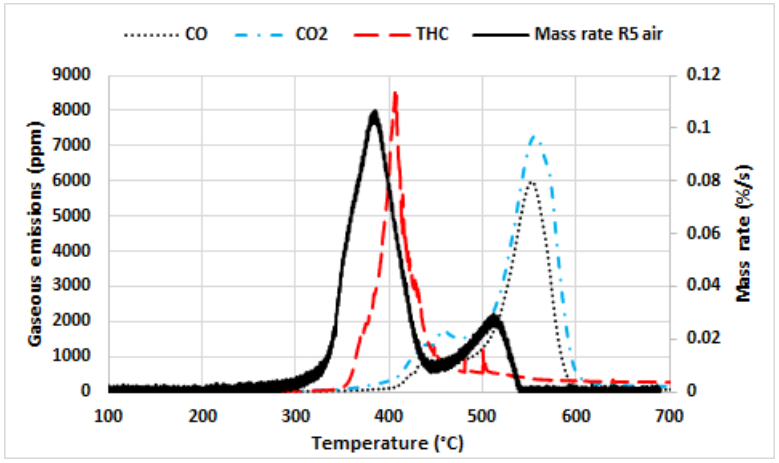

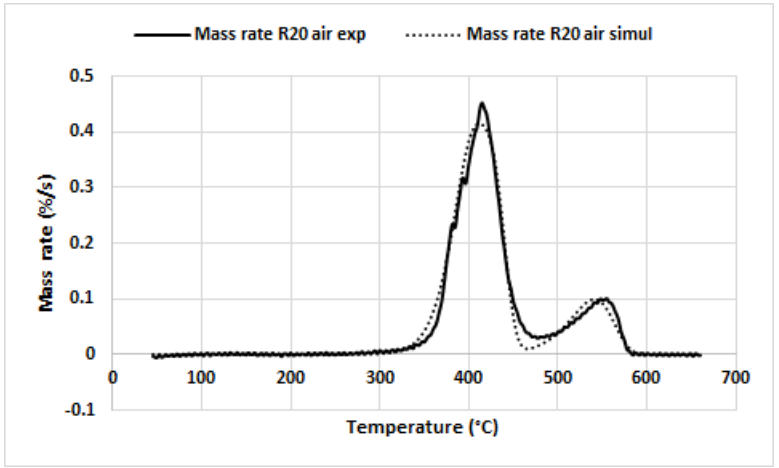

Kinetic modeling (EIPR model)